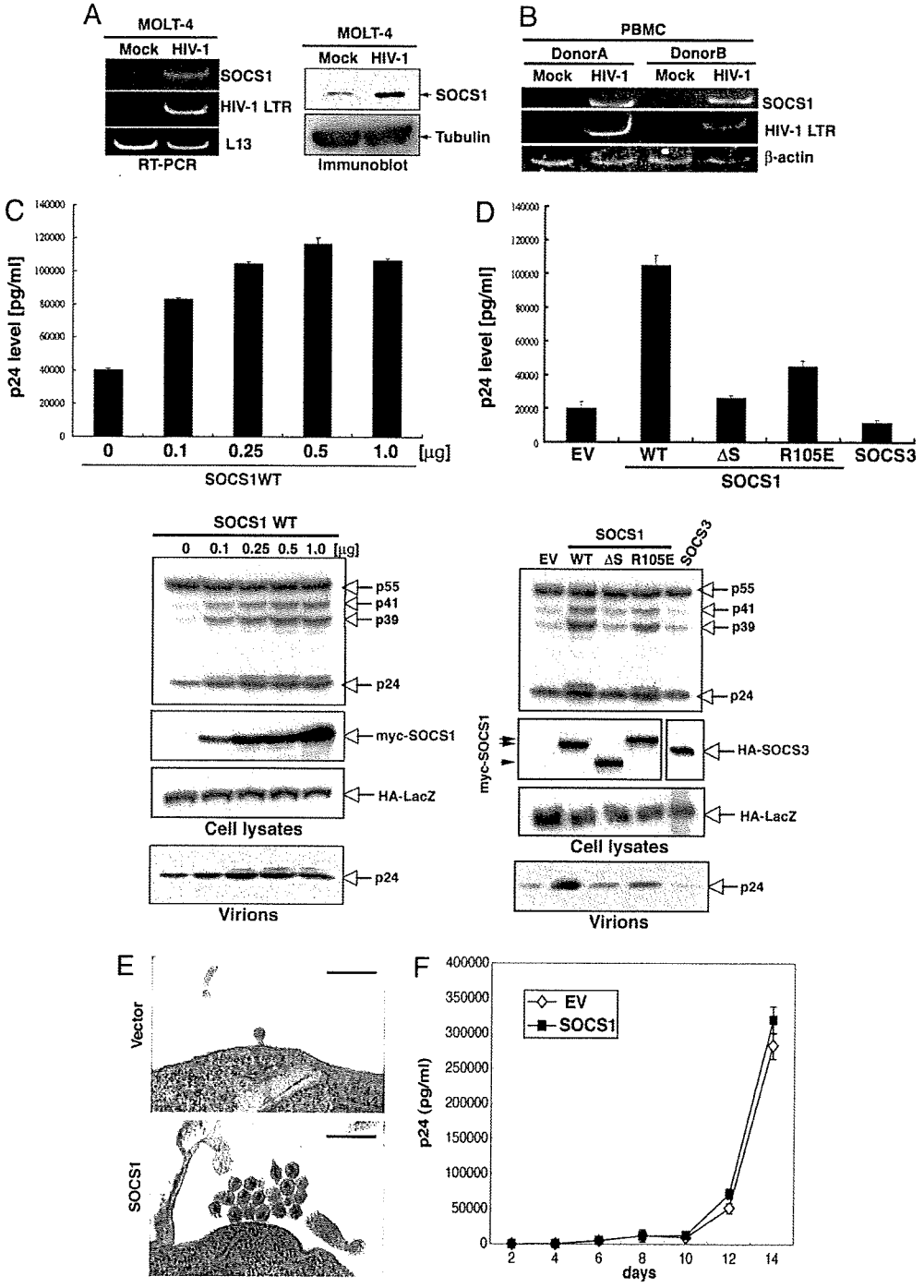

Fig. 1. SOCS1 is induced upon HIV-1 infection and enhances HIV-1 particle production. (*A*) MOLT-4 cells were mock-infected or infected with HIV-1_{NL4-3}, and then total RNA and protein extracts derived from these cells were subjected to semiquantitative RT-PCR (*Left*) and immunoblotting (*Right*), respectively. (*B*) PBMC from two healthy individuals were infected with HIV-1_{NL4-3} or were mock-infected, and SOCS1 expression was examined by semiquantitative RT-PCR. (*C*) 293T cells were transfected with pNL4-3 and cotransfected with various amounts of pcDNA-myc-SOCS1. Forty eight hours after transfection, p24 antigen release into the supernatant in each case was measured by antigen-capture ELISA (*Upper*), and the cell lysates and pelleted viruses were analyzed by immunoblotting (*Lower*). The data shown represent the mean ± SD from three independent experiments. HA-LacZ is a transfection control. (*D*) 293T cells were transfected with pNL4-3 and cotransfected with control vector, SOCS1 (WT), SOCS1ΔS (ΔSOCS box), SOCS1R105E, or SOCS3. Cell lysates and pelleted viruses were then collected after 48 h and subjected to ELISA (*Upper*) or immunoblotting (*Lower*), as described in *C*. (*E*) 293T cells cotransfected with either pNL4-3 plus control vector, or pNL4-3 plus myc-tagged SOCS1 were analyzed by TEM. Note that substantial numbers of mature virus particles can be observed in the myc-SOCS1-transfected cells. (Scale bars: 500 nm.) (*F*) Jurkat cells were infected with virions (adjusted by p24 levels) from either control vector (EV)- or SOCS1-transfected 293T cells. Supernatant p24 levels at the indicated time points were measured by ELISA.

bodies (Fig. 1*A*). In addition, *SOCS1* was found to be up-regulated also in peripheral blood mononuclear cells (PBMC) from two different individuals (following HIV infection, Fig. 1*B*).

Our initial findings that SOCS1 is induced upon HIV-1 infection prompted us to examine whether this gene product affects viral replication. We first cotransfected 293T cells with a HIV-1 infectious molecular clone, pNL4-3 (13), and also pcDNA-myc-SOCS1, and then monitored the virus production levels in the resulting supernatant. We then performed ELISA using an anti-p24 antibody and found that wild-type SOCS1 significantly increases the production of HIV-1 in the cell supernatant in a dose-dependent manner (Fig. 1*C Upper*). In contrast, neither the SH2 domain-defective mutant (R105E) nor the SOCS box deletion mutant (ΔS) of SOCS1 could promote virus production to the same levels as wild type, indicating that both domains are required for this enhancement (Fig. 1*D Upper*). Furthermore, another SOCS box protein, SOCS3, failed to augment HIV-1 replication in a parallel experiment (Fig. 1*D Upper*), indicating that the role of SOCS1 during HIV-1 replication is specific.

We next performed immunoblotting analysis using cell lysates and harvested virus particles in further parallel experiments (Fig. 1 *C* and *D Lower*). Consistent with our ELISA analysis, the expres-

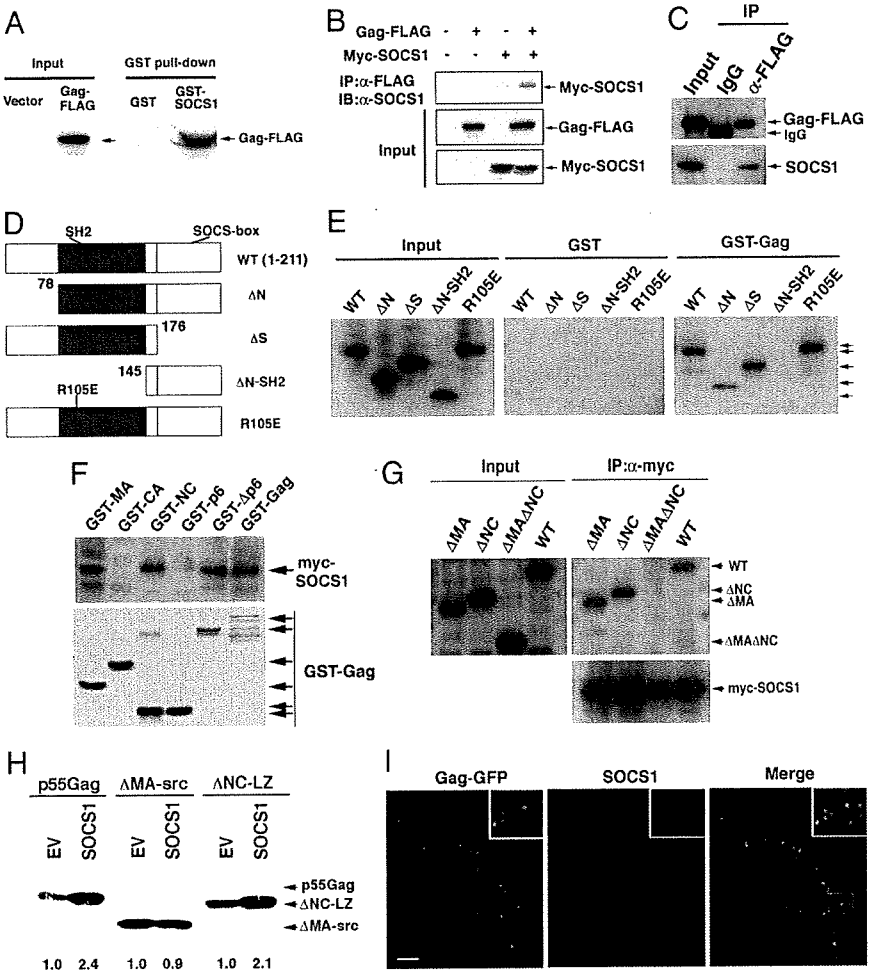

Fig. 2. SOCS1 interacts with HIV-1 Gag. (*A*) Extracts of 293T cells transfected with either empty vector or Gag-FLAG were subjected to pull-down analyses using glutathione–agarose beads with GST-SOCS1 in the presence of 10 ng/ml RNase followed by immunoblotting with anti-FLAG antibodies. (*B*) Extracts of 293T cells transiently expressing myc-SOCS1 and Gag-FLAG were subjected to immunoprecipitation (IP) with anti-FLAG monoclonal antibodies in the presence of 10 ng/ml RNase followed by immunoblotting (IB) analysis with either anti-FLAG or anti-myc polyclonal antibodies. (*C*) 293T cells were transiently transfected with Gag-FLAG, and cell lysates were then subjected to immunoprecipitation with anti-FLAG antibodies followed by immunoblotting with an antibody directed against endogenous SOCS1. (*D* and *E*) 293T cells expressing various myc-tagged SOCS1 mutants (schematically depicted in *D*) were analyzed by GST pull-down analysis with either GST or GST-Gag recombinant protein (*E*). (*F*) GST fusion proteins of the indicated regions of Gag were bound to glutathione beads and incubated with cell lysates from 293T cells expressing myc-SOCS1 in the presence of 10 ng/ml RNase followed by immunoblotting with anti-myc antibodies. (*G*) SOCS1 binds p55 Gag via either its MA or NC domains. 293T cells were transfected with myc-SOCS1 and cotransfected with Gag-FLAG, GagΔMA-FLAG, GagΔNC-FLAG, or GagΔMAΔNC-FLAG. At 24 h after transfection, cell lysates treated with 10 μg/ml RNase were subjected to coimmunoprecipitation with anti-myc monoclonal antibodies followed by immunoblotting with anti-FLAG or anti-myc polyclonal antibodies. (*H*) Functional interaction of SOCS1 with MA but not NC. 293T cells were transfected with wild-type Gag, ΔMA-src, or ΔNC-LZ (Z_{IL}-p6) and cotransfected with either control vector or SOCS1. Supernatant virus particles were then collected after 24 h and subjected to immunoblotting with anti-p24 antibody. Numerical values below the blots indicate fold induction of supernatant p55 signal intensities derived by densitometry. (*I*) Colocalization of SOCS1 with Gag. HeLa cells were transiently transfected with Gag-GFP. After 24 h, the cells were fixed, permeabilized, and immunostained with anti-SOCS1 polyclonal antibody followed by fluorescently labeled secondary antibodies before confocal microscopy. (Scale bar: 10 μm.)

sion of wild-type SOCS1, but neither its SH2 nor SOCS box mutant counterparts, resulted in a marked and dose-dependent increase in the level of intracellular Gag protein, particularly in the case of CA (p24) and intermediate cleavage products corresponding to MA-CA (p41) and CA-NC (p39). This increase was found to be accompanied by an enhanced level of HIV-1 particle production in the supernatant (Fig. 1 *C* and *D Lower*). These results together indicated that SOCS1 facilitates HIV-1 particle production in infected cells and that this role of SOCS1 requires the function of both its SH2 and SOCS box domains. For further details about SOCS1 interaction with MA and NC and SOCS1-enhanced particle production, see supporting information (SI) *Text*.

To examine the morphological aspects of HIV-1 particle production, transmission electron microscopy (TEM) was performed. 293T cells that had been cotransfected with pNL4-3, and either a control vector or a SOCS1 expression construct, were subjected to TEM analysis after fixation in glutaraldehyde. In SOCS1-transfected cells, a significantly increased number of mature virus particles was observed on the surfaces of PM compared with the control vector-transfected cells (Fig. 1*E*). There were also no obvious malformations of the virus particles in SOCS1-expressing cells, such as doublet formation or tethering to PM, which are characteristic of particle budding arrest (14) (Fig. 1*E*). Consistent with this observation, virions from SOCS1-transfected cells were found to be infectious as control viruses in Jurkat cells when the same amounts of virus were infected (Fig. 1*F*). These results together indicate that SOCS1 enhances mature and infectious HIV-1 particle formation.

To elucidate the specific step in HIV-1 production that is enhanced by SOCS1, we next performed gene reporter assays using either luciferase expression constructs under the control of wild-type HIV-LTR (pLTR-luc), or a full-length provirus vector (pNL4-3-luc) (15). Interestingly, SOCS1 overexpression was found not to affect the transcription of these reporter constructs (data not shown), indicating that SOCS1 enhances HIV-1 replication via posttranscriptional mechanisms during virus production.

SOCS1 Interacts with the HIV-1 Gag Protein. The results of our initial experiments indicated that SOCS1 enhances HIV-1 production via a posttranscriptional mechanism. We therefore next tested whether SOCS1 could bind directly to HIV-1 Gag. GST pull-down analysis using C-terminal FLAG-tagged p55 Gag (codon-optimized) and GST-fused SOCS1 revealed that p55 Gag undergoes specific coprecipitation with GST-SOCS1 (Fig. 2*A*). Furthermore, both ectopically expressed myc-tagged SOCS1 and endogenous SOCS1 were found to undergo coimmunoprecipitation with Gag-FLAG in 293T cells (Fig. 2 *B* and *C*). Additionally, GST pull-down analysis with various SOCS1 mutants, as depicted in Fig. 2*D*, further demonstrated that a mutant lacking the both N-terminal and SH2 domain (ΔN-SH2) could not bind

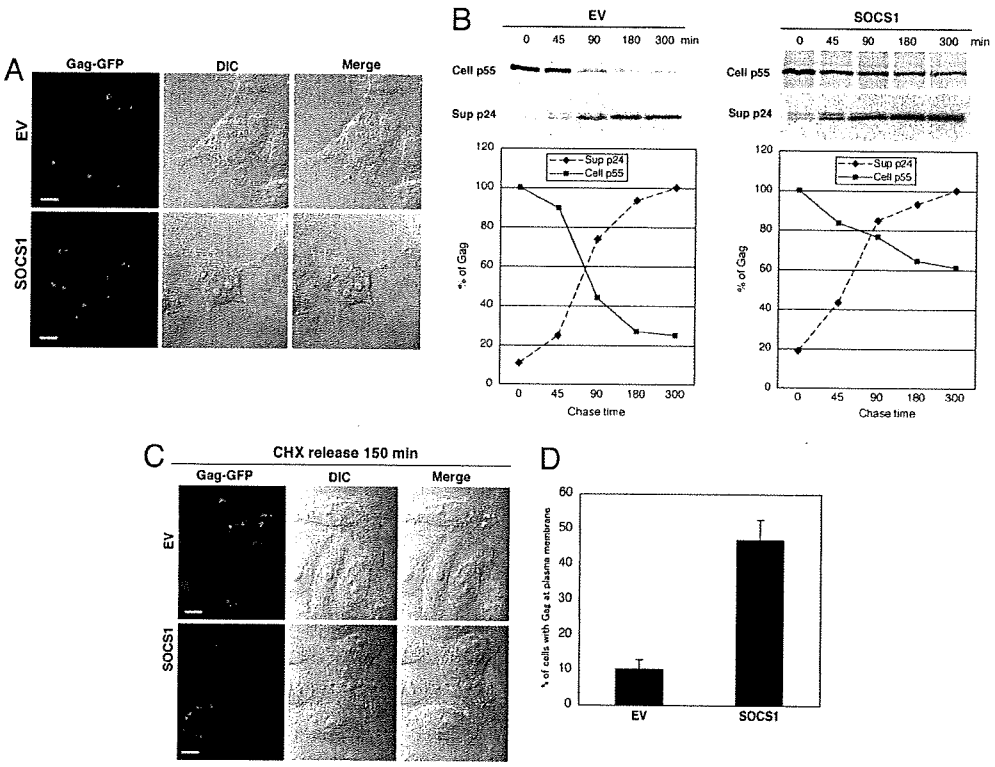

Fig. 3. SOCS1 enhances both the stability and trafficking of HIV-1 Gag. (*A*) HeLa cells cotransfected with pNL4-3 and either control vector (EV) or SOCS1 were immunostained with antibodies targeting anti-p24 (CA). Confocal microscopy with differential interference contrast (DIC) was then performed. (Scale bars: 10 μm.) (*B*) 293T cells were transfected with either a control empty vector (EV) (*Left*) or myc-SOCS1 (*Right*) and cotransfected with pNL4-3. After 48 h, cells were pulse-labeled with [^{35}S]methionine or [^{35}S]cysteine for 15 min and chased for the durations indicated. Cell lysates and pelleted supernatant virions were immunoprecipitated with anti-p24 antibodies followed by autoradiography. (*C* and *D*) HeLa cells seeded on poly-L-lysine-coated cover slides were transfected with either vector control or SOCS1. After 24 h, cells were again transfected with Gag-GFP for 3 h and then treated with 100 μg/ml CHX for 5 h to inhibit protein synthesis. This treatment was followed by incubation with fresh medium; then 150 min after the CHX release, cells were fixed and subjected to confocal microscopy (*C*). (Scale bars: 10 μm.) Cells with Gag protein on the plasma membrane were scored out of 200 transfected cells (*D*).

p55 Gag, whereas an N-terminal or a SOCS box deletion did not affect the binding of SOCS1 to Gag in 293T cells (Fig. 2*E*). This finding indicates that the SH2 domain is important for the interaction of SOCS1 with HIV-1 Gag. Interestingly, the R105E mutant of SOCS1, which disrupts the function of the SH2 domain, still binds Gag (Fig. 2*E*), indicating that the Gag–SOCS1 association is independent of the tyrosine phosphorylation of Gag, as is the case for both HPV-E7 and Vav (16, 17).

To elucidate the SOCS1-binding region of the Gag protein, GST pull-downs with various GST-fused Gag domain constructs were performed. SOCS1 was detected in glutathione bead precipitates with GST-wild-type Gag, GST-Δp6, GST-MA, and GST-NC, but not with other domain constructs (Fig. 2*F*), indicating that SOCS1 interacts with Gag via its MA and NC domains. Consistent with these results, the deletion of both the MA and NC domains of p55 Gag (ΔMAΔNC) completely abolishes its interaction with SOCS1 in coimmunoprecipitation experiments (Fig. 2*G*). Furthermore, *in vitro* analysis with purified proteins also demonstrated that SOCS1 can indeed interact with both the MA and NC regions of HIV-1 Gag in the absence of nucleic acids or other proteins (SI Fig. 5).

We next wished to determine the functional interaction domain in HIV-1 Gag through which SOCS1 functions in terms of virus-like particle production. To this end, we used a MA-deleted Gag mutant with an N-terminal myristoyl tag derived from src (ΔMA-src) (18) and also an NC-deleted Gag mutant with a GCN4 leucine zipper in place of NC, which we herein denote as ΔNC-LZ but which has been described as Z_{IL}-p6 (19). Both of these mutants have been shown still to assemble and bud (18, 19). We found that SOCS1 overexpression can still augment the particle formation of both wild-type Gag and ΔNC-LZ but not ΔMA-src (Fig. 2*H*), indicating that the functional interaction between SOCS1 and HIV-1 Gag is in fact mediated through MA.

To confirm further the direct interaction between SOCS1 and Gag in cells, we examined the intracellular localization of these two proteins. Confocal microscopy revealed that endogenous SOCS1 forms dotted filamentous structures in the cytoplasm and that Gag localizes in a very punctate pattern with SOCS1 from the perinuclear regions to the cell periphery (Fig. 2*I*). These data indicate that SOCS1 interacts with HIV-1 Gag in the cytoplasm during HIV-1 particle production.

SOCS1 Promotes both the Stability of Gag and Its Targeting to the Plasma Membrane. Because we had found from our initial data that SOCS1 increases HIV-1 particle production as a result of its direct interaction with intracellular Gag proteins, we next addressed whether SOCS1 positively regulates Gag stability and subsequent trafficking to PM. Our immunofluorescent analysis with the anti-p24 (CA) antibody initially revealed that SOCS1 overexpression increases the levels of Gag at PM when cotransfected with pNL4-3 at 48 h after transfection, although it was detected at PM in both control and SOCS1-expressing cells (Fig. 3*A*). Furthermore, the levels of cytoplasmic Gag were found to be much lower in the SOCS1-expressing cells compared with the control cells (Fig. 3*A*). These results indicate that SOCS1 enhances Gag trafficking to PM.

To examine next whether SOCS1 affects the stability and trafficking of newly synthesized Gag proteins, we performed pulse–chase analysis. This experiment revealed that SOCS1 significantly increases the stability of the intracellular p55 Gag polyprotein as well as the levels of p24 in the supernatant (Fig. 3*B*). Importantly, p24 was detectable at an earlier time point and reached maximum levels in a shorter period in the cell supernatant of SOCS1-transfected cells compared with control vector-transfected cells (Fig. 3*B*). This finding again suggests that SOCS1 facilitates the intracellular trafficking of newly synthesized Gag proteins to PM.

To confirm this hypothesis further, we performed cycloheximide (CHX) analysis with HeLa cells transfected using either vector control or SOCS1. After 24 h, cells were again transfected with Gag-GFP for 3 h and treated with CHX for 5 h to inhibit protein synthesis. Cells were then cultured in fresh medium without CHX for an additional 150 min and subjected to confocal microscopy. At

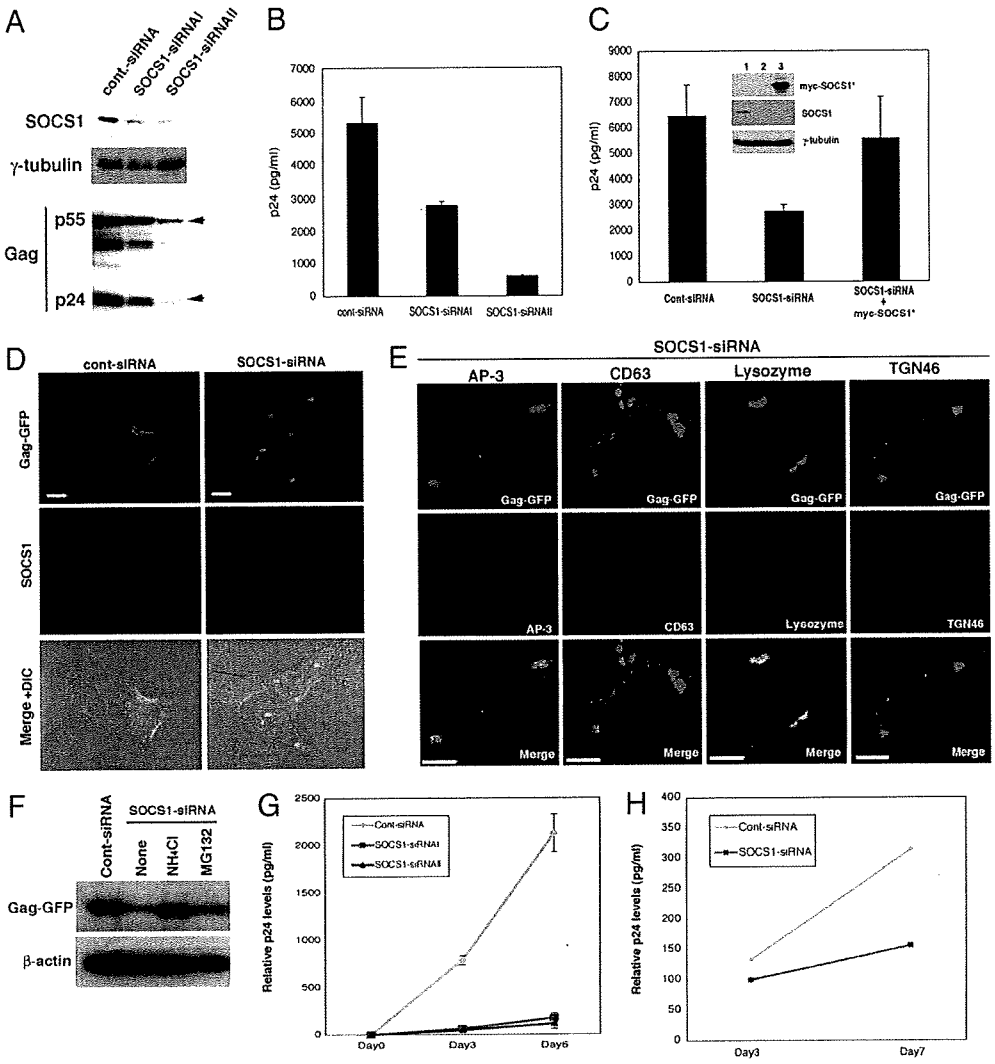

Fig. 4. The targeted inhibition of SOCS1 suppresses Gag trafficking and HIV-1 particle production and enhances Gag degradation in lysosomes. (*A* and *B*) 293T cells were transfected with either control siRNA or two different SOCS1-specific siRNAs (I or II) together with pNL4-3. At 48 h after transfection, cell lysates were subjected to immunoblotting analysis with the indicated antibodies (*A*). Cell supernatants were then subjected to ELISA analysis of p24 levels (*B*). (*C*) 293T cells were transfected with pNL4-3 and cotransfected with control-siRNA, SOCS1-siRNAI alone, or SOCS1-siRNAI plus siRNA-resistant myc-SOCS1 (myc-SOCS1*). After 48 h, cell supernatants were collected and subjected to p24 ELISA. (*Inset*) Immunoblots of the cell lysates. (*D*) HeLa cells were transfected with control or SOCS1-specific siRNA and cotransfected with GFP-Gag. At 48 h after transfection, the cells were subjected to confocal microscopy. (*E*) HeLa cells were transfected with Gag-GFP and SOCS1-siRNA constructs for 48 h. Cells were then fixed and subjected to immunofluorescent analysis with indicated antibodies followed by DAPI staining. (Scale bars: 10 mm.) (*F*) HeLa cells were transfected with Gag-GFP and cotransfected with either control-siRNA or SOCS1-siRNA. After 36 h, the cells were treated with a mock solution, 10 mM NH_4Cl or 10 μM MG132 for another 16 h. Cell were then harvested and subjected to immunoblotting analysis with anti-GFP or anti-β-actin antibodies. (*G*) Jurkat cells were infected with a retroviral vector encoding control (Cont) or two different SOCS1-specific siRNAs (I or II). After selection with puromycin, the cells were then infected with HIV-1_{NL4-3} (multiplicity of infection, 0.1), and p24 antigen levels in cell supernatant were measured by ELISA at the indicated time points. (*H*) Human primary CD4 T cells were separated from healthy donors and infected with lentivirus vectors encoding either control- or SOCS1-siRNAI. The cells were then infected with HIV-1_{NL4-3} (multiplicity of infection, 0.1), and p24 antigen levels in cell supernatant were measured by ELISA at the indicated time points.

this time point, Gag-GFP was found to localize predominantly in a perinuclear region in the control cells (Fig. 3*C*), whereas almost half of the SOCS1-transfected cells exhibited Gag-GFP localization on PM (Fig. 3*D*). These results again indicate that SOCS1 efficiently enhances the trafficking of newly synthesized Gag protein to PM.

The Targeted Disruption of SOCS1 Inhibits Gag Trafficking and HIV-1 Particle Production. To delineate further the role of SOCS1 in the trafficking of Gag and in subsequent HIV-1 particle production, we depleted cellular SOCS1 by siRNA. The significant depletion of SOCS1 expression by two different SOCS1-specific siRNA constructs was confirmed by immunoblotting analysis (Fig. 4 *A* and *B*). Significantly, in cells cotransfected with pNL4-3 and SOCS1-specific siRNAs, both HIV-1 particle release and the levels of intracellular Gag protein are significantly decreased compared with the control cells (Fig. 4 *A* and *B*). Furthermore, the effects of SOCS1-siRNA on the inhibition of HIV-1 particle production was diminished by reexpression with a codon-optimized SOCS1 construct that is resistant to these siRNAs (Fig. 4*C*), indicating that the SOCS1 siRNA suppression of HIV-1 particle production depends on the availability of endogenous SOCS1.

Consistent with these observations, immunofluorescent analysis further revealed that the expression of SOCS1-siRNA dramatically inhibits Gag trafficking such that Gag proteins accumulate in the perinuclear regions as large solid aggregates, as has been reported (20) (Fig. 4*D*). This finding indicates that SOCS1 plays an essential role in the Gag trafficking from perinuclear clusters to PM. Interestingly, these discrete perinuclear clusters of Gag were found to colocalize with lysosome markers, lysozyme, and partly with AP-3, but neither with the late endosome MVB marker CD63 nor the *trans*-Golgi marker TGN46, indicating that Gag is targeted for degradation by lysosomes when the function of SOCS1 is inhibited (Fig. 4*E*). In support of this notion, the levels of intracellular Gag were found to be significantly increased by treatment with a lysosome inhibitor NH_4Cl but not by a proteasome inhibitor MG132 in SOCS1-siRNA cells (Fig. 4*F*), further indicating that the perinuclear clusters of Gag will undergo lysosomal degradation rather than proteasomal degradation when optimal Gag transport to PM is suppressed by the inhibition of SOCS1.

We next addressed whether targeted SOCS1 inhibition would affect HIV-1 particle production in human T cells. The effect of SOCS1 depletion was clearly evident in both HIV-1_{NL4-3}-infected

Jurkat cells and human primary CD4$^+$ T cells, which demonstrated pronounced decreases in virus particle production in SOCS1-siRNA-expressed cells compared with the controls (Fig. 4 *G* and *H*). These results together indicate that the specific inhibition of SOCS1 suppresses the optimal trafficking of Gag to PM, resulting in the degradation of Gag in lysosomes, which in turn leads to the efficient and reproducible inhibition of HIV-1 particle production in various types of human cells.

Discussion

In this work, we report that SOCS1 is an inducible host factor during HIV-1 infection and plays a key role in the late stages of the viral replication pathway via an IFN-independent mechanism (SI Fig. 6). These results represent evidence that SOCS1 is a potent host factor that facilitates HIV-1 particle production via posttranscriptional mechanisms.

SOCS1 has been shown to be a suppressor of several cytokine signaling pathways, and like all SOCS family members it has a central SH2 domain and a conserved C-terminal domain known as the SOCS box (21, 22). Structure–function analyses have further demonstrated that the SOCS1 SH2 domain is required for the efficient binding of its substrates (23, 24). Indeed, our current analyses have also revealed that the SH2 domain of SOCS1 is required for its interaction with the HIV-1 Gag protein. We have shown from our present data that the SOCS box is also required for SOCS1 to function during HIV-1 particle production.

The SOCS box-mediated function of SOCS1 is chiefly exerted via its ubiquitin ligase activity (21, 25). Biochemical binding studies have shown that the SOCS box of SOCS1 interacts with the elongin BC complex, a component of the ubiquitin/proteasome pathway that forms an E3 ligase with Cul2 (or Cul5) and Rbx-1 (21, 26, 27). We show from our current experiments that the SOCS box is required for HIV-1 particle production, indicating the involvement of the ubiquitin/proteasome pathway. However, it is still unknown whether SOCS1 promotes the ubiquitination of Gag and, if so, whether the mono- or poly-ubiquitination of Gag would affect its trafficking and protein stability. Further studies will be necessary to clarify the biological significance of Gag ubiquitination.

Perlman and Resh (20) recently reported that newly synthesized Gag first appears to be diffusely distributed in the cytoplasm, accumulates in perinuclear clusters, passes transiently through a MVB-like compartment, and then traffics to PM. Consistent with these observations, our current work also shows that Gag is accumulated at perinuclear clusters as solid aggregates when its targeting to PM is impaired because of the SOCS1 inhibition.

Another aspect of SOCS1 function during HIV-1 infection was proposed recently. Song *et al.* (28) reported that SOCS1-silenced dendritic cells broadly induce the enhancement of HIV-1 Env-specific CD8$^+$ cytotoxic T lymphocytes and CD4$^+$ T helper cells as well as an antibody response. The induction of the SOCS1 gene in HIV-1 infected cells might therefore disrupt a specific intracellular immune response to HIV-1 in infected host cells.

Based on the strong evidence that we present in our current work that SOCS1 positively regulates the late stages of HIV replication, we conclude that SOCS1 is likely to be a valuable therapeutic target not only for future treatments of AIDS and related diseases, but also for a postexposure prophylaxis against disease in HIV-1-infected individuals.

Materials and Methods

Antibodies and Fluorescent Reagents. Antibodies and fluorescent reagents were obtained from the following sources. Anti-CD63, anti-AP-3, anti-myc (A-14), and anti-SOCS1 (H-93) were from Santa Cruz Biotechnology. Anti-SOCS1 was from Zymed Laboratories. Anti-FLAG (M2) and anti-HA (12CA5) were from Sigma and Roche Diagnostics, respectively. Anti-HIV-p24 (Dako; Cytomation), anti-STAT1, and anti-phospho-STAT1 (Y701) were from BD Transduction Laboratories. Sheep polyclonal anti-TGN46 was from GeneTex.

Plasmid Constructs. Expression constructs for SOCS1 have been described in ref. 29. GST fusion constructs with specific regions derived from the codon-optimized *gag* were generated (MA, CA, NC, p6, Δp6, full-length Gag) by cloning into pGEX-2T (GE Healthcare Bio-Sciences) as described in ref. 30. For retrovirus-mediated siRNA expression, pSUPER.retro.puro vector was digested, as described in ref. 31, with the following sequences: SOCS1-siRNAI, TCGAGCTGCTGGAGCACTA; SOCS1-siRNAII, GGCCAGAACCTTCCTCCTCTT; control siRNA, TCGTATGTTGTGTGGAATT.

Electron Microscopy. Transfected 293T cells were fixed with 2.5% glutaraldehyde and subjected to TEM, as described (14, 32).

ACKNOWLEDGMENTS. We thank Dr. H Gottlinger (University of Massachusetts) for providing plasmids. This work was supported in part by grants from the Ministry of Education, Culture, Sports, Science, and Technology of Japan and Human Health Science of Japan.

1. Sorin M, Kalpana GV (2006) *Curr HIV Res* 4:117–130.
2. Freed EO (2004) *Trends Microbiol* 12:170–177.
3. Peterlin BM, Trono D (2003) *Nat Rev Immunol* 3:97–107.
4. Trkola A (2004) *Curr Opin Microbiol* 7:555–559.
5. Freed EO (1998) *Virology* 251:1–15.
6. Adamson CS, Jones IM (2004) *Rev Med Virol* 14:107–121.
7. VerPlank L, Bouamr F, LaGrassa TJ, Agresta B, Kikonyogo A, Leis J, Carter CA (2001) *Proc Natl Acad Sci USA* 98:7724–7729.
8. Garrus JE, von Schwedler UK, Pornillos OW, Morham SG, Zavitz KH, Wang HE, Wettstein DA, Stray KM, Cote M, Rich RL, *et al.* (2001) *Cell* 107:55–65.
9. Strack B, Calistri A, Craig S, Popova E, Gottlinger HG (2003) *Cell* 114:689–699.
10. Dong X, Li H, Derdowski A, Ding L, Burnett A, Chen X, Peters TR, Dermody TS, Woodruff E, Wang JJ, *et al.* (2005) *Cell* 120:663–674.
11. Alroy I, Tuvia S, Greener T, Gordon D, Barr HM, Taglicht D, Mandil-Levin R, Ben-Avraham D, Konforty D, Nir A, *et al.* (2005) *Proc Natl Acad Sci USA* 102:1478–1483.
12. Ryo A, Suzuki Y, Ichiyama K, Wakatsuki T, Kondoh N, Hada A, Yamamoto M, Yamamoto N (1999) *FEBS Lett* 462:182–186.
13. Adachi A, Gendelman HE, Koenig S, Folks T, Willey R, Rabson A, Martin MA (1986) *J Virol* 59:284–291.
14. Demirov DG, Ono A, Orenstein JM, Freed EO (2002) *Proc Natl Acad Sci USA* 99:955–960.
15. Chang TL, Mosoian A, Pine R, Klotman ME, Moore JP (2002) *J Virol* 76:569–581.
16. De Sepulveda P, Okkenhaug K, Rose JL, Hawley RG, Dubreuil P, Rottapel R (1999) *EMBO J* 18:904–915.
17. Kamio M, Yoshida T, Ogata H, Douchi T, Nagata Y, Inoue M, Hasegawa M, Yonemitsu Y, Yoshimura A (2004) *Oncogene* 23:3107–3115.
18. Gallina A, Mantoan G, Rindi G, Milanesi G (1994) *Biochem Biophys Res Commun* 204:1031–1038.
19. Accola MA, Strack B, Gottlinger HG (2000) *J Virol* 74:5395–5402.
20. Perlman M, Resh MD (2006) *Traffic* 7:731–745.
21. Alexander WS (2002) *Nat Rev Immunol* 2:410–416.
22. Marine JC, Topham DJ, McKay C, Wang D, Parganas E, Stravopodis D, Yoshimura A, Ihle JN (1999) *Cell* 98:609–616.
23. Narazaki M, Fujimoto M, Matsumoto T, Morita Y, Saito H, Kajita T, Yoshizaki K, Naka T, Kishimoto T (1998) *Proc Natl Acad Sci USA* 95:13130–13134.
24. Yasukawa H, Misawa H, Sakamoto H, Masuhara M, Sasaki A, Wakioka T, Ohtsuka S, Imaizumi T, Matsuda T, Ihle JN, *et al.* (1999) *EMBO J* 18:1309–1320.
25. Tyers M, Rottapel R (1999) *Proc Natl Acad Sci USA* 96:12230–12232.
26. Kamizono S, Hanada T, Yasukawa H, Minoguchi S, Kato R, Minoguchi M, Hattori K, Hatakeyama S, Yada M, Morita S, *et al.* (2001) *J Biol Chem* 276:12530–12538.
27. Kamura T, Burian D, Yan Q, Schmidt SL, Lane WS, Querido E, Branton PE, Shilatifard A, Conaway RC, Conaway JW (2001) *J Biol Chem* 276:29748–29753.
28. Song XT, Evel-Kabler K, Rollins L, Aldrich M, Gao F, Huang XF, Chen SY (2006) *PLoS Med* 3:e11.
29. Ryo A, Suizu F, Yoshida Y, Perrem K, Liou YC, Wulf G, Rottapel R, Yamaoka S, Lu KP (2003) *Mol Cell* 12:1413–1426.
30. Morikawa Y, Kishi T, Zhang WH, Nermut MV, Hockley DJ, Jones IM (1995) *J Virol* 69:4519–4523.
31. Ryo A, Uemura H, Ishiguro H, Saitoh T, Yamaguchi A, Perrem K, Kubota Y, Lu KP, Aoki I (2005) *Clin Cancer Res* 11:7523–7531.
32. Nagashima Y, Nishihira H, Miyagi Y, Tanaka Y, Sasaki Y, Nishi T, Imaizumi K, Aoki I, Misugi K (1996) *Cancer* 77:799–804.

MAJOR ARTICLE

Interleukin-4–Transgenic hu-PBL-SCID Mice: A Model for the Screening of Antiviral Drugs and Immunotherapeutic Agents against X4 HIV-1 Viruses

Kazu Okuma,[1] Reiko Tanaka,[1] Tomoyuki Ogura,[2] Mamoru Ito,[2] Sei Kumakura,[3] Mikiro Yanaka,[3] Masako Nishizawa,[4] Wataru Sugiura,[4] Naoki Yamamoto,[4] and Yuetsu Tanaka[1]

[1]Department of Immunology, Graduate School and Faculty of Medicine, University of the Ryukyus, Okinawa, [2]Central Institute for Experimental Animals, Kanagawa, and [3]Kureha Corporation and [4]National Institute of Infectious Diseases, Tokyo, Japan

CXCR4-tropic (X4) human immunodeficiency virus type 1 (HIV-1) does not efficiently infect and replicate in severe combined immunodeficiency (SCID) mice reconstituted with human peripheral blood mononuclear cells, termed "hu-PBL-SCID mice," due to, at least in part, relatively low levels of expression of the CXCR4 coreceptor. To overcome this limitation, interleukin (IL)–4–transgenic hu-PBL-SCID mice were derived that spontaneously synthesized human IL-4, which has been shown to enhance CXCR4 expression and promote X4 virus infection in vitro. Experiments reported here show that (1) synthesis of human IL-4 in vivo augmented CXCR4 expression on human CD4$^+$ lymphocytes and importantly led to productive infection of not only X4 HIV-1_{NL4-3} but also multidrug-resistant primary clinical isolates and that (2) the in vivo infection could be significantly blocked by the administration of a CXCR4 antagonist. Altogether, IL-4–transgenic hu-PBL-SCID mice provide a useful model for X4 HIV-1 study and testing/screening of anti-X4 viral drugs.

HIV-1 isolates enter target cells primarily after binding to the CD4 receptor and via the CXCR4 and CCR5 coreceptors [1–5] and are classified into X4 and R5 strains, respectively [6]. The X4 isolates are frequently implicated in the decline of peripheral CD4$^+$ T cell counts characteristic of the late stage of HIV-1 infection proceeding to the development of AIDS [7].

hu-PBL-SCID mice have been extensively used as a small animal model to study HIV-1 pathogenesis [8–14]. Results from a previous study showed that, although infection of human peripheral blood mononuclear cell (PBMC)–reconstituted hu-PBL-SCID mice with a predominantly R5 HIV-1 caused intensive CD4$^+$ T cell depletion, infection of similarly reconstituted mice with the same infectious dose of an X4 HIV-1 resulted in little or no CD4$^+$ T cell depletion [11]. Thereafter, it was noted that this limitation of X4 HIV-1 infection was due, at least in part, to a decrease in the intensity of CXCR4 expression on CD4$^+$ T cells [13]. Thus, it was reasoned that the pathogenic effects of the X4 HIV-1 strains in the hu-PBL-SCID mice might be related to the relative levels of the expression of HIV-1 coreceptor (the state of activation/differentiation) on human CD4$^+$ T cells at the time of infection in these mice. This limitation has to date restricted our ability to use this mouse model for understanding the mechanisms of X4 HIV-1 pathogenesis and for the evaluation of candidate therapeutics against X4 viruses. These findings prompted us to seek alternative strategies for the development of an improved hu-PBL-SCID mouse system that is permissive for infection/replication of X4 isolates.

Human interleukin (IL)–4 has been shown to specifically enhance the cell-surface expression of CXCR4 on

Received 1 May 2007; accepted 11 July 2007; electronically published 4 December 2007.

Potential conflicts of interest: none reported.

Presented in part: First International Workshop on Humanized Mice, Tokyo, 11–12 October 2006 (abstract P-15); 14th Conference on Retroviruses and Opportunistic Infections, Los Angeles, 25–28 February 2007 (abstract 496).

Financial support: Health and Labor Science Research Grant (Research on Publicly Essential Drugs and Medical Devices) from the Ministry of Health, Labor, and Welfare of Japan (grant H16-soyaku-004).

Reprints or correspondence: Dr. Kazu Okuma, Dept. of Immunology, Graduate School and Faculty of Medicine, University of the Ryukyus, Uehara 207, Nishihara-cho, Nakagami-gun, Okinawa 903-0215, Japan (kokuma@med.u-ryukyu.ac.jp).

The Journal of Infectious Diseases 2008; 197:134–41

0022-1899/2008/19701-0021$15.00

DOI: 10.1086/524303

resting peripheral blood T cells [15]. Furthermore, it has been reported that human IL-4 plays an important role in rendering $CD4^+$ T cells susceptible to X4 HIV-1 infection via enhanced cell-surface expression of the CXCR4 coreceptor in vitro [15–17].

In efforts to overcome the limitation inherent with the use of hu-PBL-SCID mice for the study of X4 HIV-1 as described above, we developed an IL-4–transgenic immunodeficient mouse model that consistently secreted readily detectable serum levels of human IL-4. We show here that X4 isolates readily infect/replicate in this mouse model but not in wild-type (wt) non–IL-4–transgenic mice and that this model can now be exploited for the rapid evaluation of the therapeutic efficacy of new anti-X4 HIV-1 agents in vivo.

METHODS

IL-4–producing mice. Two strains of human IL-4–transgenic immunodeficient mice were bred on the C.B-17-*scid* [18] and BALB/cA-Rag2$^{-/-}\gamma_c^{-/-}$ (dKO) genetic background mice [19, 20] at the Central Institute for Experimental Animals (CIEA) as follows. PBMCs were isolated from a healthy human volunteer and activated in vitro with pokeweed mitogen. RNA was prepared from these PBMCs, and then cDNA was synthesized by reverse-transcriptase polymerase chain reaction (PCR). Human IL-4 cDNA was amplified from the cDNA using one set of primers: 5'-CCCGGGATCGTTAGCTTCTCCTGATAAAA-3' and 5'-GCGGCCGCTATTCAGCTCGAACACTTTGAAT-3'. The product was inserted into the PCR2.1 vector by use of the TA cloning kit (Invitrogen) and the insert sequenced. After confirmation of the sequence, IL-4 cDNA was inserted into pCMVb with a CMV promoter (Invitrogen). To produce transgenic mice, a DNA fragment containing the CMV promoter, IL-4 cDNA, and Poly(A) regions was excised with *Xho*I and *Hind*III sites of pCMVb and microinjected into the pronuclei of fertilized eggs from the 2 strains (C.B-17-*scid* and BALB/cA-dKO) of mice. These eggs were subsequently transplanted into oviducts of pseudopregnant foster recipient mice. The offspring mice were screened to confirm the insertion of the transgene into the genome by PCR, and serum from these mice was screened for levels of human IL-4 by ELISA with a commercial kit (BD). The IL-4 transgene–hemizygous mice were maintained by mating them with wt mice with the same genetic background in the specific-pathogen–free (SPF) facility of the CIEA. The mice were transferred to the SPF and biosafety level 3 facilities of the Institute for Animal Experiments, University of the Ryukyus, and were used for further experiments. The experimental protocols were approved by the Institutional Animal Care and Use Committee on the basis of the Regulation for Animal Experimentation of the CIEA and University of the Ryukyus before the initiation of the study.

Viruses. X4 HIV-1_{NL4-3} was obtained as described elsewhere [14]. Fourteen multidrug-resistant (MDR) HIV-1 clinical isolates were obtained from HIV-1–infected patients who had been treated with highly active antiretroviral therapy (HAART). The viruses were propagated in PBMCs stimulated with phytohemagglutinin (PHA; Sigma), IL-2 (National Institutes of Health AIDS Research and Reference Reagent Program), and IL-4 (Peprotec). Three isolates from these MDR isolates that efficiently grew in the activated cells were selected for further experiments. The titers of virus stocks were determined by end-point titration using a 2-fold limiting dilution of the stock and in vitro PHA-activated human PBMCs, and the infectious units (IU) were calculated.

CXCR4 antagonist. The synthesis and purification of the CXCR4 antagonist KRH-1636 were performed at Kureha Corporation as described elsewhere [21]. As a control, the carrier tartrate was used in parallel.

Transplantation and infection. The control (wt) and the IL-4–transgenic C.B-17-*scid* mice were depleted of NK cells by the intraperitoneal (ip) injection of 0.5–1.0 mg of anti–mouse IL-2R β (TMβ-1) [22] per animal. The IL-4–transgenic and the control BALB/cA-dKO mice do not require TMβ-1 treatment because they lack NK cells [19, 20]. PBMCs were isolated from healthy human donors. Groups of 2–4-month-old IL-4–transgenic mice from each of the 2 background strains and their corresponding non–IL-4–transgenic wt mice were injected ip with PBMCs 3 days later. Groups of mice were challenged 24 h later ip with mock, HIV-1_{NL4-3}, or MDR isolates (2000 IU/500 μL/animal). For the experiments using the CXCR4 antagonist, groups of mice were administered 0.1 mL of 10 mmol/L KRH-1636, the tartrate carrier or saline ip at 1 h before and 1 day after virus infection. At 6–8 days after infection, the mice were killed, their blood was obtained by cardiocentesis, and human lymphocytes were collected from the peritoneal lavage fluids. The serum samples were assayed for levels of human IL-4 by use of an ELISA kit (R&D Systems). The human lymphocytes were analyzed using flow cytometry as described below. The remaining cells were cultured in RPMI 1640 medium (Sigma) supplemented with fetal calf serum and IL-2. The peritoneal lavage fluids, serum samples, and lymphocyte culture supernatants were examined for levels of p24 by use of an ELISA kit (Zepto Metrix).

Flow cytometry analysis. Cell samples to be analyzed by flow cytometry were initially incubated with normal human IgG for blocking of the Fc receptors. For cell-surface staining, aliquots of cells were then stained with Cy5-labeled anti-CD4 (OKT4) and phycoerythrin-labeled anti-CXCR4 (12G5; Dako) or with Cy5-labeled anti-CD3 (OKT3). For intracellular staining, after CD3 staining the aliquots of cells were fixed, permeabilized, and incubated with fluorescein isothiocyanate–labeled anti–HIV-1 Gag p24 (2C2; Y.T. et al., unpublished data). Stained samples were analyzed on a FACSCalibur flow cytometer, using Cell Quest software (BD Pharmingen). Aliquots of cells stained

Table 1. Expression of human CD4, CXCR4, and intracellular HIV-1 p24 in cells from X4 HIV-1–infected hu-PBL-SCID mice.

Category	X4 HIV-1 infection	Mice, no.	$CD4^+$ T cells, %	*P*	$CXCR4^+CD4^+$ T cells, %	*P*	$p24^+$ T cells, %	*P*
C.B-17-*scid* mice								
Control	NL4-3	6	22.1 ± 8.3	<.001	45.2 ± 4.7	<.001	0.1 ± 0.1	NS
IL-4 transgenic	NL4-3	6	66.3 ± 9.0		65.5 ± 6.1		0.1 ± 0.1	
BALB/cA-dKO mice								
Control	NL4-3	5	35.9 ± 5.1	<.01	32.6 ± 1.4	<.001	0.2 ± 0.1	<.05
IL-4 transgenic	NL4-3	3	57.4 ± 8.3		68.2 ± 3.9		3.2 ± 1.2	

NOTE. Cells in peritoneal lavage fluid from control and interleukin (IL)–4–transgenic hu-PBL-SCID mice on either the C.B-17-*scid* or BALB/cA-dKO background were labeled with appropriate monoclonal antibodies and analyzed by flow cytometry, as described in Methods. Analyzed data are shown as mean ± SD values. NS, not significant. The indicated *P* values for the comparison of control vs. transgenic mice for each category are based on Student's *t* test.

with or without each of the antibodies described above were used as controls for the purposes of establishing gates and for the determination of the frequency of positive cells.

Statistical analysis. Data obtained by flow cytometry were analyzed by Student's *t* test with GraphPad Prism (version 4.0c for Mac OS X; GraphPad Software).

RESULTS

Production of human IL-4 in IL-4–transgenic mice. Efforts to construct the IL-4–transgenic mice constitutively synthesizing human IL-4 finally led to the establishment of mice on each of the 2 immunodeficient backgrounds expressing either high or low serum levels of human IL-4 (data not shown). On the basis of preliminary data obtained on the efficiency of virus replication, all subsequent experiments were done using only the 2 strains with high serum IL-4 expression levels. We assayed for levels of human IL-4 in the serum from the $IL\text{-}4^+$ hu-PBL-SCID mice and the wt hu-PBL-SCID mice on either the C.B-17-*scid* or BALB/cA-dKO background after infection with X4 HIV-$1_{NL4\text{-}3}$. Serum from each of the IL-4–transgenic mice on either background contained significant levels of human IL-4 (~800–1800 pg/mL), whereas serum from the control mice on the same background showed nondetectable levels of human IL-4. These data demonstrate that the human IL-4 synthesized by the IL-4–transgenic mice is generated from the transgene but not from the human PBMCs transplanted in these mice.

Effect of human IL-4 on the levels of human CXCR4 and CD4 expression by cells transplanted into mice. Since human IL-4 has been previously documented to enhance the expression of CXCR4 in vitro, experiments were done to examine the expression of human CXCR4 on transplanted $CD4^+$ cells in the peritoneal lavage fluids from HIV-$1_{NL4\text{-}3}$–infected $IL\text{-}4^+$ hu-PBL-SCID mice and control hu-PBL-SCID mice on either the C.B-17-*scid* or BALB/cA-dKO background. There did not appear to be any detectable difference in the absolute amounts of cells recovered from the peritoneal lavage fluids from the IL-4–positive or IL-4–negative hu-PBL-SCID mice on either background (data not shown). Flow cytometry analysis demonstrated that the frequency of human $CD4^+$ cells from the IL-4–transgenic C.B-17-*scid* or BALB/cA-dKO mice was significantly higher than that from the control mice (table 1). As expected, there was a marked increase in the frequency of CXCR4-expressing $CD4^+$ cells from the IL-4–transgenic mice on either genetic background relative to that from the control mice (figure 1*A* and table 1). Thus, these data indicate that human IL-4 produced endogenously is functional in vivo in terms of its ability to enhance human CXCR4 expression on $CD4^+$ cells transplanted into the mice.

Increased frequency of X4 HIV-1–infected cells from IL-4–transgenic hu-PBL-SCID mice. Since the constitutive synthesis of human IL-4 in IL-4–transgenic hu-PBL-SCID mice resulted in the enhanced expression of X4 HIV-1 receptors (human CXCR4/CD4) on the transplanted cells, we reasoned that such cells were likely to be more permissive to the infection and replication of X4 HIV-1. We thus challenged the IL-4–transgenic hu-PBL-SCID mice and control hu-PBL-SCID mice bred on the C.B-17-*scid* or BALB/cA-dKO mice with HIV-$1_{NL4\text{-}3}$. Cells obtained from the peritoneal lavage fluids were analyzed for cell-surface expression of human CD3 (since HIV-1 down-modulates CD4 expression) and the presence of intracellular p24. As seen in figure 1*B* and table 1, although very few if any $CD3^+$ cells from the control or IL-4–transgenic C.B-17-*scid* mice showed p24 expression, there was a >10-fold increase in the frequency of $CD3^+$ T cells that expressed p24 from the IL-4–transgenic BALB/cA-dKO mice relative to the control mice. These data suggest that, while transgene-induced human IL-4 increases the frequency of $CD4^+CXCR4^+$ T cells transplanted into both the C.B-17-*scid* and the BALB/cA-dKO mice, only the latter demonstrates increased sensitivity to X4 HIV-1 infection and replication, at least when this assay is used (see below).

High production of X4 HIV-1 in the culture supernatants of cells from IL-4–transgenic hu-PBL-SCID mice. In an effort

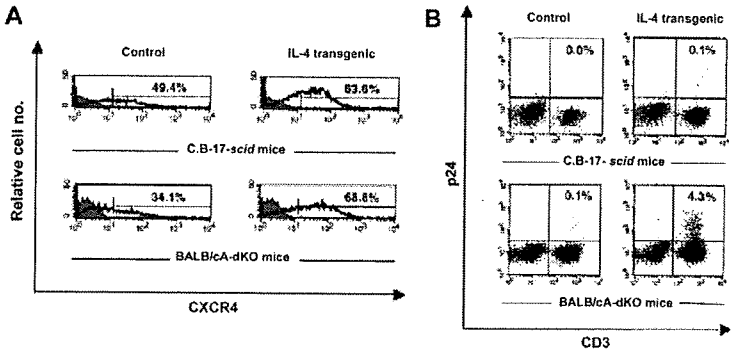

Figure 1. Enhancement of the expression of CXCR4 coreceptor and facilitation of X4 HIV-1 infection and replication in hu-PBL-SCID mice by in vivo production of human interleukin (IL)–4. Groups of hu-PBL-SCID mice, generated from IL-4–transgenic and nontransgenic (control) mice on either the C.B-17-*scid* or BALB/cA-dKO background, were injected intraperitoneally with HIV-1_{NL4-3} at ~24 h after peripheral blood mononuclear cell (PBMC) reconstitution. Six to eight days later, peritoneal lavage fluids were harvested from mice in each group, and cells were collected from the fluids by density-gradient centrifugation. *A*, Cells analyzed for the frequency and mean density of human CXCR4 expression on $CD4^+$ cells by flow cytometry. Data for analyzed cells are depicted by a thick line, and the background control profile is depicted by a thin line and gray shading. The nos. above the bars represent the percentage of positive cells. Data shown are representative of mice in each group from 3 independent experiments. *B*, HIV-1 infectivity. Cells were subjected to flow cytometry after cell-surface CD3 and intracellular p24 staining. Analyzed data are depicted as dot plots. The nos. in the graphs indicate the percentage of $CD3^+p24^+$ cells. Data displayed are representative of mice in each group from 3 independent experiments.

to determine the reason for our failure to detect levels of intracellular p24 in the IL-4–transgenic mice on the C.B-17-*scid* background and to further support the above finding, peritoneal lavage fluids were collected from mock- or HIV-1_{NL4-3}–infected $IL\text{-}4^+$ hu-PBL-SCID mice and, for purposes of control, the HIV-1_{NL4-3}–infected non–IL-4–transgenic mice on the C.B-17-*scid* background. The cells were isolated from the peritoneal lavage fluids, and an aliquot was analyzed for the frequency and the relative density of human CXCR4/CD4; the remaining aliquot was cultured in vitro. In addition, the peritoneal lavage fluids and the culture supernatants of cells at days 1–3 after culture were assayed for levels of p24 production. As displayed in table 2, although the frequency of $CXCR4^+CD4^+$ cells in the IL-4–transgenic mice was significantly higher than that in the nontransgenic mice, the mean fluorescence intensity (MFI) of CXCR4 expressed by the $CD4^+$ T cells from these mice was not increased compared with the control (because of an increase in the frequency of $CXCR4^+CD4^+$ cells with relatively low MFI; see figure 1*A*). Analysis of levels of synthesized p24 demonstrated marked differences, as shown in figure 2. Thus, although the amounts of p24 produced were modest in the peritoneal lavage fluids and the cell-culture supernatants from HIV-1–infected control mice, the levels of p24 produced by those from HIV-1–infected IL-4–transgenic mice were strikingly higher (15,429, 11,844, 1696, and 53 pg/mL in the supernatants on day 3) (mean, 48.9 vs. 7255 pg/mL; >100-fold increase). Although the levels of p24 produced by one of the IL-4–transgenic mice (mouse 12) were similar to those in the control mice, this was likely due to the much lower relative level of human IL-4 (354 pg/mL in serum) produced by mouse 12 than those from the other 3 IL-4–transgenic mice (4227, 6313, and 2356 pg/mL in serum). The present data not only document the fact that the cells from these

Table 2. Effect of the CXCR4 antagonist KRH-1636 on the expression of human CXCR4 by $CD4^+$ cells from X4 HIV-1–infected interleukin (IL)–4–transgenic hu-PBL-SCID mice.

C.B-17-*scid* mice	X4 HIV-1 Infection	CXCR4 antagonist	Mice, no.	$CXCR4^+CD4^+$ T cells, %	*P*	CXCR4 on $CD4^+$ T cells, MFI	*P*
Control	NL4-3	Mock	4	45.5 ± 9.3	<.05[a]	73.7 ± 36.0	NS[a]
IL-4 transgenic	NL4-3	Mock	4	66.7 ± 7.4	NS[b]	73.1 ± 6.2	<.05[b]
IL-4 transgenic	NL4-3	KRH-1636	4	63.0 ± 4.2	...	62.2 ± 4.8	...

NOTE. Control or IL-4–transgenic hu-PBL-SCID mice on the C.B-17-*scid* background infected with X4 HIV-1_{NL4-3} were administered mock KRH-1636 or real KRH-1636. Cells isolated from the peritoneal lavage fluid from the mice in each group were labeled with appropriate monoclonal antibodies and subjected to flow cytometry, as described in Methods. Data analyzed are displayed as mean ± SD values. MFI, mean fluorescence intensity; NS, not significant. The indicated *P* values are based on Student's *t* test.

[a] For the comparison between control mice and IL-4–transgenic mice that received a mock CXCR4 antagonist.

[b] For the comparison between IL-4–transgenic mice that received a mock CXCR4 antagonist and IL-4–transgenic mice that received KRH-1636.

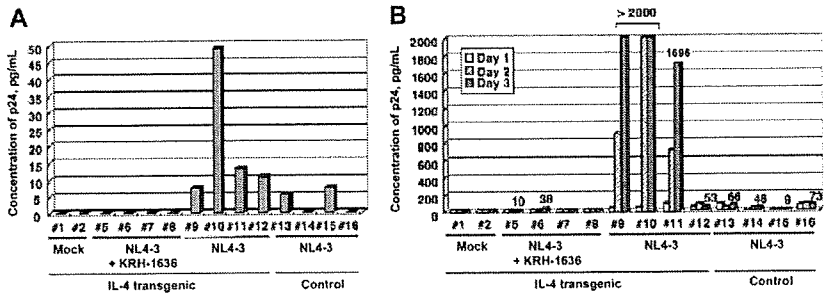

Figure 2. Efficient infection of interleukin (IL)–4–producing hu-PBL-SCID mice with X4 laboratory strain and an inhibitory effect of the CXCR4 antagonist KRH-1636 on infection. Twelve IL-4–transgenic and 4 nontransgenic (control) hu-PBL-SCID mice were generated on the C.B-17-*scid* background. Among them, 8 IL-4–transgenic and 4 control mice were infected intraperitoneally (ip) with the X4 laboratory strain (HIV-1_{NL4-3}) and 4 IL-4–transgenic mice were mock-infected at 1 day after engraftment. To evaluate the effect of KRH-1636, this drug was administered ip twice, at 1 h before and 1 day after infection of 4 IL-4–transgenic mice (NL4-3 + KRH-1636). At 8 days after infection, peritoneal lavage fluids were obtained from the mice in each group. Cells were isolated from the fluids and cultured in IL-2–containing medium. Levels of HIV-1 p24 in the peritoneal lavage fluids *(A)* and culture supernatants at days 1–3 after incubation *(B)* were quantitated for infectivity and replication efficiency by ELISA. With regard to the data on mock-infected mice, only 2 of 4 representative data are presented. The nos. listed above the bars in the graph indicate levels of HIV-1 p24 when it was detectable on day 3 (most of the values were <200 pg/mL, and select samples showed values of >2000 pg/mL). Pound signs (#) indicate mouse nos. Results shown are representative of 3 independent experiments.

IL-4–transgenic C.B-17-*scid* mice are susceptible but also demonstrate that the virus from such cells is replication competent. In addition, these findings suggest that the use of intracellular p24 levels is not a sensitive enough technique and that data using the intracellular p24 assay need to be carefully evaluated. These data also indicate that the IL-4–transgenic hu-PBL-SCID mice provide a powerful model for the study of X4 HIV-1 infection independently of the genetic background of the mice.

Inhibitory effect of the CXCR4 antagonist on infection of IL-4–transgenic hu-PBL-SCID mice with the X4 laboratory strain. In an effort to further validate that the CXCR4 coreceptor was indeed used by the X4 HIV-1 virus in the IL-4–transgenic hu-PBL-SCID mice, we used the X4 virus-entry inhibitor, CXCR4 antagonist KRH-1636. Thus, the IL-4–transgenic hu-PBL-SCID mice on the C.B-17-*scid* background were infected with X4 laboratory strain HIV-1_{NL4-3} and were either mock treated or treated with KRH-1636, and the peritoneal lavage fluids, cells in fluids, and cell-culture supernatants were examined as described above. As shown in table 2, the frequency of $CXCR4^+CD4^+$ cells in KRH-1636–treated IL-4–transgenic mice was marginally lower than that in mock-treated IL-4–transgenic mice. In addition, the MFI of CXCR4 expression by the $CD4^+$ T cells was clearly reduced by KRH-1636 administration. Importantly, treatment with KRH-1636 almost completely blocked X4 HIV-1 infection in these IL-4–transgenic mice (figure 2). These data indicate that X4 HIV-1 infection in transgenic mice is CXCR4 dependent and that our mouse model can be used to develop and test new anti-X4 HIV-1 drugs in vivo.

Therapeutic effect of KRH-1636 on the infection of IL-4–transgenic hu-PBL-SCID mice with MDR clinical isolates. The appearance of MDR HIV-1 clinical isolates has been and continues to be one of the growing problems in a significant number of patients receiving HAART and seriously limits the use of the antiviral drugs that are currently available. Thus, the development of novel adjunct or alternative therapeutics is an urgent need. Since treated patients tend to harbor significantly higher levels of either dual/mixed or X4 viruses [23] and since MDR isolates are not usually refractory to new treatment with drugs from classes that have not been used previously in patients from which the viruses were derived, we finally wanted to examine the effect of KRH-1636 on MDR HIV-1 infection in IL-4–transgenic hu-PBL-SCID mice. For this experiment, we used the IL-4–transgenic BALB/cA-dKO mice instead of the IL-4–transgenic C.B-17-*scid* mice, because the former seems more permissive to X4 HIV-1 infection than the latter, as described above. Before the in vivo study, we confirmed that the in vitro infection by 3 MDR clinical isolates could be inhibited with KRH-1636 (more than ~90% inhibition at the 5-μmol/L level). Thus, groups of IL-4–transgenic hu-PBL-SCID mice were infected with a mixture of these selected MDR isolates containing equal IU of each virus and treated with KRH-1636 or the tartrate carrier control. Thereafter, the cells obtained from the peritoneal lavage fluids were analyzed for the expression of cell-surface human CD4, CD3, and intracellular p24. The serum, peritoneal lavage fluids, and supernatants following in vitro culture of the cells for 24 h were assayed for levels of p24 production. Flow cytometry analysis after CD4 staining demonstrated a significant decline in $CD4^+$ T cells in 2 (mouse 7 and mouse 8) of 4 control-treated mice (figure 3*A*; top profile shows data from 1 of these 2 mice), which was likely due to MDR HIV-1 pathogenesis. However, importantly, no detectable depletion of $CD4^+$ T cells was observed in any of 4 KRH-1636–treated mice (figure 3*A*; bottom profile). As summarized in table 3, the difference in the frequency of $CD4^+$ T cells between the control-treated mice and the

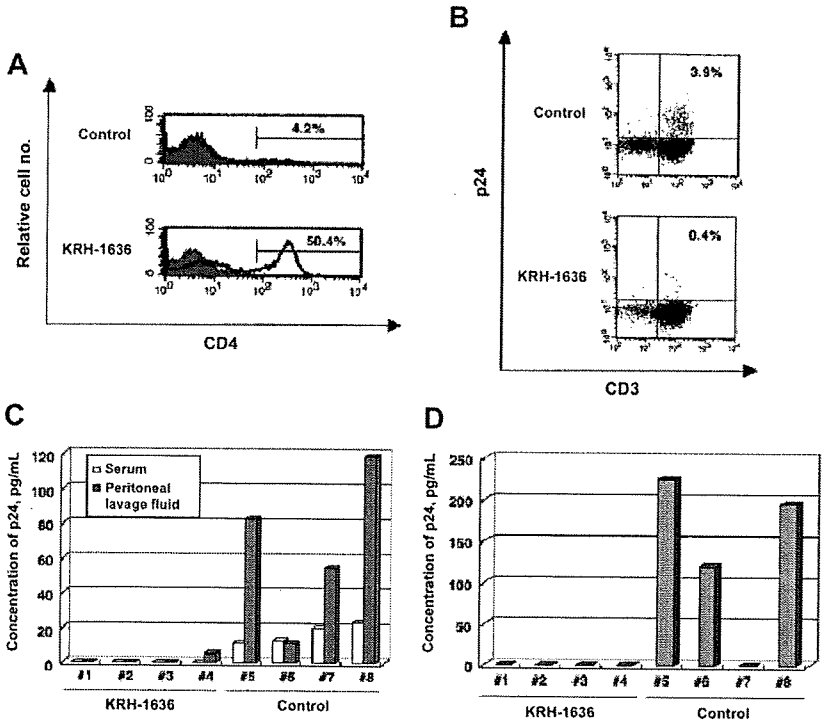

Figure 3. Prophylactic effect of KRH-1636 on infection and pathogenesis by multidrug-resistant (MDR) HIV-1 clinical isolates. Eight interleukin (IL)–4–transgenic hu-PBL-SCID mice (BALB/cA-dKO) were infected intraperitoneally (ip) with a mixture of MDR HIV-1 clinical isolates at 1 day after human peripheral blood mononuclear cell transfer. In an effort to assess the effect of KRH-1636 on HIV-1 infection, this agent or tartrate (control drug) was administered to 4 mice per group ip twice, at 1 h before infection and 1 day after infection. At 7 days after infection, serum and peritoneal lavage fluids were harvested from mice in each group, and cells were collected from the fluids. *A*, Cells examined for human CD4 expression by cell-surface staining and standard flow cytometry. Representative data from a single mouse from the control-treated or the KRH-1636–treated HIV-1–infected mice are shown. The frequency of $CD4^+$ T cells is depicted by a thick line, and the background control is depicted by a thin line with gray shading. The nos. above the bars indicate the percentage of positive cells. *B*, Aliquot of the peritoneal lavage cells analyzed by flow cytometry for the frequency of $CD3^+$ T cells that were positive for the intracellular presence of HIV-1 p24. Representative data of cells from the control-treated and the KRH-1636–treated HIV-1–infected mice are shown. The nos. in the graphs indicate the percentage of $CD3^+p24^+$ cells. *C*, Concentrations of p24 in serum and peritoneal lavage fluid. Concentrations were determined by ELISA to quantify MDR HIV-1 infection and replication efficiency. Pound signs (#) indicate mouse nos. *D*, Levels of in vitro p24 production. The remaining cells were cultured in a microtiter plate containing $IL\text{-}2^+$ medium for ~24 h, and the culture supernatants obtained were assayed for levels of in vitro p24 production by ELISA. Pound signs (#) indicate mouse nos. Results shown are representative of 3 similar independent experiments.

KRH-1636–treated mice was not significant. However, the MFI of CD4 expression was significantly decreased in the control-treated mice (229.3 vs. 296.3; $P < .05$). Results of CD3/p24 staining showed that the frequency of $CD3^+p24^+$ cells was markedly inhibited in the KRH-1636–treated mice, compared with that in the carrier-treated control mice (figure 3*B* and table 3). Furthermore, levels of HIV-1 p24 in the serum samples, peritoneal lavage fluids, and culture supernatants from the KRH-

Table 3. Effect of KRH-1636 on infection and pathogenesis by multidrug-resistant (MDR) HIV-1 clinical isolates in interleukin (IL)–4–transgenic hu-PBL-SCID mice.

BALB/cA-dKO mice	X4 HIV-1 infection	CXCR4 antagonist	Mice, no.	$CD4^+$ T cells, %	*P*	$CD4^+$ T cells, MFI	*P*	$p24^+$ T cells, %	*P*
IL-4 transgenic	MDR	Control	4	14.7 ± 11.9	NS	229.3 ± 33.0	<.05	3.2 ± 0.8	<.01
IL-4 transgenic	MDR	KRH-1636	4	31.3 ± 15.7		296.3 ± 25.2		0.8 ± 0.7	

NOTE. IL-4–transgenic hu-PBL-SCID mice on the BALB/cA-dKO background were infected with MDR HIV-1 clinical isolates and administered tartrate (control) or KRH-1636. Cells in peritoneal lavage fluid from the mice in each group were stained with appropriate monoclonal antibodies and analyzed by flow cytometry, as described in Methods. Data shown here are mean ± SD values. MFI, mean fluorescence intensity; NS, not significant. The indicated *P* values for the comparison between control mice and mice that received KRH-1636 are based on Student's *t* test.

1636–treated HIV-1–infected mice were almost completely reduced relative to those in the control mice (figure 3*C* and 3*D*). Note that the failure to detect the in vitro production of p24 in mouse 7 might result from depletion of $CD4^+$ T cells (figure 3*D*). These data demonstrate that the CXCR4 antagonist KRH-1636 has a marked degree of prophylactic effect on infection with pathogenic MDR clinical isolates in vivo.

DISCUSSION

Humanized mice that have served as valuable small animal models include the SCID-hu Thy/Liv mouse [24–28]. This mouse model, generated by implanting human hematopoietic tissues (human fetal thymus/liver) under the kidney capsule, has been used for the study of HIV-1 and is known for permissiveness to X4 HIV-1 infection [26–28]. However, the use of this model is limited by the fact that the implants are of human fetal organ origins that are not easily available. On the other hand, the hu-PBL-SCID mouse model provides another surrogate in vivo HIV-1 infection assay system. Although this model has led to a number of successful studies of HIV-1 [8–14], there was still a limitation in that it was difficult to demonstrate X4 HIV-1 infection and replication in such mice. Thus, to add extra value to the use of this mouse system for the study of HIV-1, in the present study we developed novel human IL-4–transgenic hu-PBL-SCID mice that enable CXCR4-using HIV-1 strains to efficiently infect and replicate in these mice.

Human IL-4 has low homology with murine IL-4 both at the gene and protein levels, accounting for the lack of cross-reactivity of this cytokine in the 2 species in vitro [29–32]. Results of the experiments reported here indicate that the high efficiency of X4 HIV-1 infection in the IL-4–transgenic hu-PBL-SCID mice was, at least in part, secondary to enhanced expression of viral receptors induced by human IL-4 synthesized endogenously. Interestingly, although there was no apparent increase in the number of cells recovered from the engrafted transgenic mice, there was a significant increase in the number of $CD4^+$ T cells recovered (1.5–3-fold). It is thus possible that the other cell lineages migrate from the peritoneal cavity to other tissues of the mice, resulting in enrichment of the $CD4^+$ T cell lineage. However, further studies of other tissues are needed to clarify this issue. Furthermore, our preliminary experiments indicate that the IL-4–transgenic hu-PBL-SCID mice remain permissive to R5 strain infection (data not shown).

In this report, we created 2 types of novel hu-PBL-SCID mice by transplanting human PBMCs into IL-4–transgenic C.B-17-*scid* and BALB/cA-dKO mice. The data obtained show that hu-PBL-SCID mice using the IL-4–producing BALB/cA-dKO mice appeared more permissive to X4 HIV-1 infection than did those using the IL-4–producing C.B-17-*scid* mice, at least as determined by the presence of intracellular p24. Although the reasons for this difference remain to be determined, it should be noted that, whereas the BALB/cA-dKO mice were derived by double mutation with defects in both the recombinase-activating gene 2 (Rag-2) and the gene encoding the γ_c chain of select cytokine receptors [19, 20], the C.B-17-*scid* mice have only the Rag-2 mutation [18]. Thus, although the Rag-2 mutation prevents the normal maturation of T and B lymphocytes, the γ_c chain mutation abrogates the expression of functional receptors for IL-2 and other cytokines, preventing the expansion of lymphocytes, including NK cells, which play an important role in the innate immune response such as nonspecific rejection of xenogeneic grafts. It is thus possible that the C.B-17-*scid* mice maintain a low but significant residual level of NK cell function, which may play a role in the difference noted above even though they were administered significant levels of anti–IL-2Rβ antibody. Since the BALB/cA-dKO mice are completely deficient in NK cell lineage and function, they are more immunodeficient than the C.B-17-*scid* mice, suggesting that the level and type of immunodeficiency in the BALB/cA-dKO mice may facilitate better engraftment and more efficient viral infection and propagation within these mice. These select defects of the BALB/cA-dKO mice might render the IL-4–transgenic mouse model on this background more valuable and ideal for studies of X4 HIV-1.

Acknowledgments

We thank the National Institutes of Health AIDS Research and Reference Reagent Program and M. Sasaki for supplying interleukin-2 and technical support, respectively. We are also grateful to Prof. Aftab Ansari for his critical reading of the manuscript and for his helpful discussion about and suggestions for the manuscript.

References

1. Feng Y, Broder CC, Kennedy PE, Berger EA. HIV-1 entry cofactor: functional cDNA cloning of a seven-transmembrane, G protein-coupled receptor. Science **1996**; 272:872–7.
2. Alkhatib G, Combadiere C, Broder CC, et al. CC CKR5: a RANTES, MIP-1alpha, MIP-1beta receptor as a fusion cofactor for macrophage-tropic HIV-1. Science **1996**; 272:1955–8.
3. Berson JF, Long D, Doranz BJ, Rucker J, Jirik FR, Doms RW. A seven-transmembrane domain receptor involved in fusion and entry of T-cell-tropic human immunodeficiency virus type 1 strains. J Virol **1996**; 70: 6288–95.
4. Deng H, Liu R, Ellmeier W, et al. Identification of a major co-receptor for primary isolates of HIV-1. Nature **1996**; 381:661–6.
5. Doranz BJ, Rucker J, Yi Y, et al. A dual-tropic primary HIV-1 isolate that uses fusin and the beta-chemokine receptors CKR-5, CKR-3, and CKR-2b as fusion cofactors. Cell **1996**; 85:1149–58.
6. Berger EA, Doms RW, Fenyo EM, et al. A new classification for HIV-1. Nature **1998**; 391:240.
7. Xiao L, Rudolph DL, Owen SM, Spira TJ, Lal RB. Adaptation to promiscuous usage of CC and CXC-chemokine coreceptors in vivo correlates with HIV-1 disease progression. AIDS **1998**; 12:F137–43.
8. Mosier DE. Adoptive transfer of human lymphoid cells to severely immunodeficient mice: models for normal human immune function, autoimmunity, lymphomagenesis, and AIDS. Adv Immunol **1991**; 50:303–25.
9. Mosier DE, Gulizia RJ, Baird SM, Wilson DB, Spector DH, Spector SA. Human immunodeficiency virus infection of human-PBL-SCID mice. Science **1991**; 251:791–4.

10. Torbett BE, Picchio G, Mosier DE. hu-PBL-SCID mice: a model for human immune function, AIDS, and lymphomagenesis. Immunol Rev **1991**; 124:139–64.
11. Mosier DE, Gulizia RJ, MacIsaac PD, Torbett BE, Levy JA. Rapid loss of CD4+ T cells in human-PBL-SCID mice by noncytopathic HIV isolates. Science **1993**; 260:689–92.
12. Rizza P, Santini SM, Logozzi MA, et al. T-cell dysfunctions in hu-PBL-SCID mice infected with human immunodeficiency virus (HIV) shortly after reconstitution: in vivo effects of HIV on highly activated human immune cells. J Virol **1996**; 70:7958–64.
13. Fais S, Lapenta C, Santini SM, et al. Human immunodeficiency virus type 1 strains R5 and X4 induce different pathogenic effects in hu-PBL-SCID mice, depending on the state of activation/differentiation of human target cells at the time of primary infection. J Virol **1999**; 73:6453–9.
14. Yoshida A, Tanaka R, Murakami T, et al. Induction of protective immune responses against R5 human immunodeficiency virus type 1 (HIV-1) infection in hu-PBL-SCID mice by intrasplenic immunization with HIV-1-pulsed dendritic cells: possible involvement of a novel factor of human $CD4^+$ T-cell origin. J Virol **2003**; 77:8719–28.
15. Jourdan P, Abbal C, Noraz N, et al. IL-4 induces functional cell-surface expression of CXCR4 on human T cells. J Immunol **1998**; 160:4153–7.
16. Tanaka Y, Koyanagi Y, Tanaka R, Kumazawa Y, Nishimura T, Yamamoto N. Productive and lytic infection of human CD4+ type 1 helper T cells with macrophage-tropic human immunodeficiency virus type 1. J Virol **1997**; 71:465–70.
17. Suzuki Y, Koyanagi Y, Tanaka Y, et al. Determinant in human immunodeficiency virus type 1 for efficient replication under cytokine-induced $CD4^+$ T-helper 1 (Th1)- and Th2-type conditions. J Virol **1999**; 73:316–24.
18. Bosma GC, Custer RP, Bosma MJ. A severe combined immunodeficiency mutation in the mouse. Nature **1983**; 301:527–30.
19. Traggiai E, Chicha L, Mazzucchelli L, et al. Development of a human adaptive immune system in cord blood cell-transplanted mice. Science **2004**; 304:104–7.
20. Berges BK, Wheat WH, Palmer BE, Connick E, Akkina R. HIV-1 infection and CD4 T cell depletion in the humanized $Rag2^{-/-}\gamma c^{-/-}$ (RAG-hu) mouse model. Retrovirology **2006**; 3:76.
21. Ichiyama K, Yokoyama-Kumakura S, Tanaka Y, et al. A duodenally absorbable CXC chemokine receptor 4 antagonist, KRH-1636, exhibits a potent and selective anti-HIV-1 activity. Proc Natl Acad Sci USA **2003**; 100:4185–90.
22. Tanaka T, Kitamura F, Nagasaka Y, Kuida K, Suwa H, Miyasaka M. Selective long-term elimination of natural killer cells in vivo by an anti-interleukin 2 receptor beta chain monoclonal antibody in mice. J Exp Med **1993**; 178:1103–7.
23. Hunt PW, Harrigan PR, Huang W, et al. Prevalence of CXCR4 tropism among antiretroviral-treated HIV-1–infected patients with detectable viremia. J Infect Dis **2006**; 194:926–30.
24. Goldstein H, Pettoello-Mantovani M, Katopodis NF, Kim A, Yurasov S, Kollmann TR. SCID-hu mice: a model for studying disseminated HIV infection. Semin Immunol **1996**; 8:223–31.
25. McCune JM. Animal models of HIV-1 disease. Science **1997**; 278:2141–2.
26. Aldrovandi GM, Feuer G, Gao L, et al. The SCID-hu mouse as a model for HIV-1 infection. Nature **1993**; 363:732–6.
27. Berkowitz RD, Alexander S, Bare C, et al. CCR5- and CXCR4-utilizing strains of human immunodeficiency virus type 1 exhibit differential tropism and pathogenesis in vivo. J Virol **1998**; 72:10108–17.
28. Bonyhadi ML, Rabin L, Salimi S, et al. HIV induces thymus depletion in vivo. Nature **1993**; 363:728–32.
29. Yokota T, Otsuka T, Mosmann T, et al. Isolation and characterization of a human interleukin cDNA clone, homologous to mouse B-cell stimulatory factor 1, that expresses B-cell- and T-cell-stimulating activities. Proc Natl Acad Sci USA **1986**; 83:5894–8.
30. Bonsch D, Kammer W, Lischke A, Friedrich K. Species-specific agonist/antagonist activities of human interleukin-4 variants suggest distinct ligand binding properties of human and murine common receptor gamma chain. J Biol Chem **1995**; 270:8452–7.
31. Idzerda RL, March CJ, Mosley B, et al. Human interleukin 4 receptor confers biological responsiveness and defines a novel receptor superfamily. J Exp Med **1990**; 171:861–73.
32. Morrison BW, Leder P. A receptor binding domain of mouse interleukin-4 defined by a solid-phase binding assay and in vitro mutagenesis. J Biol Chem **1992**; 267:11957–63.

Research article

Open Access

Low-intensity pulsed ultrasound activates the phosphatidylinositol 3 kinase/Akt pathway and stimulates the growth of chondrocytes in three-dimensional cultures: a basic science study

Ryohei Takeuchi[1], Akihide Ryo[2,3], Noriko Komitsu[1], Yuko Mikuni-Takagaki[4], Atsuko Fukui[1], Yuta Takagi[5], Toshihiko Shiraishi[5], Shin Morishita[5], Yoshiyuki Yamazaki[1], Ken Kumagai[1], Ichiro Aoki[3] and Tomoyuki Saito[1]

[1]Department of Orthopaedic Surgery, Yokohama City University School of Medicine, 3-9 Fukuura, Kanazawa-ku, Yokohama City, Kanagawa 236-0004, Japan
[2]First Research Group, AIDS Research Center, National Institute of Infectious Diseases, 4-7-1 Gagkuen, Musashimurayama, Tokyo 208-0011, Japan
[3]Department of Pathology, Yokohama City University School of Medicine, 3-9 Fukuura, Kanazawa-ku, Yokohama City, Kanagawa 236-0004, Japan
[4]Department of Functional Biology, Kanagawa Dental College, 82 Inaokachyo, Yokosuka City, Kanagawa 238-8580, Japan
[5]Department of Environment and Information Sciences, Yokohama National University Graduate School, 79-5 Tokiwadai, Hodogaya-ku, Yokohama City, Kanagawa 240-851, Japan

Corresponding author: Ryohei Takeuchi, take0822@hotmail.com

Received: 22 Nov 2007 Revisions requested: 21 Dec 2007 Revisions received: 6 Jun 2008 Accepted: 11 Jul 2008 Published: 11 Jul 2008

Arthritis Research & Therapy 2008, **10**:R77 (doi:10.1186/ar2451)
This article is online at: http://arthritis-research.com/content/10/4/R77

Abstract

Introduction The effect of low-intensity pulsed ultrasound (LIPUS) on cell growth was examined in three-dimensional-cultured chondrocytes with a collagen sponge. To elucidate the mechanisms underlying the mechanical activation of chondrocytes, intracellular signaling pathways through the Ras/mitogen-activated protein kinase (MAPK) and the integrin/phosphatidylinositol 3 kinase (PI3K)/Akt pathways as well as proteins involved in proliferation of chondrocytes were examined in LIPUS-treated chondrocytes.

Methods Articular cartilage tissue was obtained from the metatarso-phalangeal joints of freshly sacrificed pigs. Isolated chondrocytes mixed with collagen gel and culture medium composites were added to type-I collagen honeycomb sponges. Experimental cells were cultured with daily 20-minute exposures to LIPUS. The chondrocytes proliferated and a collagenous matrix was formed on the surface of the sponge. Cell counting, histological examinations, immunohistochemical analyses and western blotting analysis were performed.

Results The rate of chondrocyte proliferation was slightly but significantly higher in the LIPUS group in comparison with the control group during the 2-week culture period. Western blot analysis showed intense staining of type-IX collagen, cyclin B_1 and cyclin D_1, phosphorylated focal adhesion kinase, and phosphorylated Akt in the LIPUS group in comparison with the control group. No differences were detected, however, in the MAPK, phosphorylated MAPK and type-II collagen levels.

Conclusion LIPUS promoted the proliferation of cultured chondrocytes and the production of type-IX collagen in a three-dimensional culture using a collagen sponge. In addition, the anabolic LIPUS signal transduction to the nucleus via the integrin/phosphatidylinositol 3-OH kinase/Akt pathway rather than the integrin/MAPK pathway was generally associated with cell proliferation.

Introduction

The degenerative abrasion of cartilage tissue due to aging and a malalignment of the lower extremities causes osteoarthritis. Moreover, articular cartilage is a tissue that is difficult to

3D = three-dimensional; DMEM = Dulbecco's modified Eagle's medium; FAK = focal adhesion kinase; FBS = fetal bovine serum; LIPUS = low-intensity pulsed ultrasound; MAPK= mitogen-activated protein kinase; PBS = phosphate-buffered saline; PCNA = proliferating cell nuclear antigen; PI3K= phosphatidylinositol 3-OH kinase.

regenerate once damaged. Many attempts have therefore been made to achieve regeneration of damaged cartilage tissue. Conservative treatments include physiotherapy, such as quadriceps muscle training, or the intra-articular injection of hyaluronic acid. The regeneration of normal cartilage tissue, however, has not yet been achieved [1]. The elements that promote the regeneration of cartilage include growth factors [2], soluble mediators [3], corrections of any malalignment and mechanical stimulation [4-6].

Surgical treatments include a high tibial osteotomy, the microfracture method, transplantation of osteocartilaginous plugs [7], and transplantation of cultured cartilage [8]. During the transplantation of cultured cartilage, a key part of the procedure is the *in vitro* preparation of high-quality cartilage tissue prior to transplantation [9]. Mechanical stimulation is one of the essential factors that promotes the differentiation and proliferation of intact chondrocytes as well as *in vitro* cultures for transplantation. Various methods of mechanical stimulation of chondrocytes have been reported, such as loading with hydrostatic pressure [10], the application of tensile stress against the culture scaffold [11], oscillation using a vibrator [12] and low-intensity pulsed ultrasound (LIPUS) [13-15].

The matrix surrounding the chondrocytes also plays an important role in the proliferation and survival of chondrocytes. Through this extracellular matrix, chondrocytes receive various kinds of extracellular information such as mechanical signals and hormonal mediators. Mechanical stimulation has been reported to activate chondrocytes and to promote their synthesis of the extracellular matrix. Few reports have focused on the signal transmission, however, which results in chondrocyte activation. To characterize these mechano-transduction pathways in chondrocytes, we have previously established a new three-dimensional (3D) culture system, which forms a tissue architecture similar to the structure of articular cartilage tissue *in vivo* [12]. The effects of vibration on chondrocytes were previously examined in this system, and the involvement of a mechano-transduction pathway via the integrin/mitogen-activated protein kinase (MAPK) pathway and of another signaling pathway via β-catenin was evaluated. Although many previous studies reported that osteoblasts are activated by LIPUS, which has been widely used in clinical settings to accelerate the process of fracture healing, its practical use for cartilage repair in a clinical setting is so far limited [16-18].

The present study demonstrates that the combination of the 3D chondrocyte culturing technique with LIPUS not only promotes the production of type-IX collagen, but also significantly increases the number of chondrocytes. In addition, the results indicate the potential involvement of the integrin/phosphatidylinositol 3-OH kinase (PI3K)/Akt pathway downstream of LIPUS exposure, rather than the integrin/MAPK/MAPK kinase pathway, which is generally involved in the induction of cellular proliferation.

Materials and methods

Cell cultures

Articular cartilage tissue was obtained from the metatarsophalangeal joints of freshly slaughtered 6-month-old pigs in a slaughterhouse. Articular cartilage slices were cut into smaller pieces, and the cartilage specimens were washed well in PBS (pH 7.4) and digested with 0.25% trypsin–ethylenediamine tetraacetic acid (Gibco, Grand Island, NY, USA) for 20 minutes. The resultant chondrocyte preparations were washed again with PBS to remove the trypsin, and were then incubated for about 8 hours in Dulbecco's modified Eagle's medium (DMEM; Gibco) supplemented with 0.1% type-II collagenase (Worthington Biochemical Co., Lakewood, OH, USA), 10% heat-inactivated FBS (Equitech-Bio, Inc., Kerrville, TX, USA) and antibiotics. The chondrocytes were subsequently isolated and washed with culture medium, collected by centrifugation (2,000 rpm, 37°C, 5 min), and then mixed with 0.2% atelocollagen gel (type-I collagen derived from bovine tendons; Koken Co., Tokyo, Japan) containing culture medium (DMEM; Gibco).

Twenty-four-well plates containing type-I honeycomb collagen sponges (discs with a diameter of 15 mm and thickness of 2 mm; Koken Co.) at the bottom of each well were used as 3D carriers of the chondrocyte culture [19]. Chondrocytes in the atelocollagen gel and also chondrocytes in the culture medium composites were added to each sponge and were incubated at 37°C for 1 hour. The final cell density was adjusted to 2×10^6 cells/well/ml [12]. After the collagen sponge and cell–collagen gel composites became stiff, they were then incubated with 2 ml complete DMEM in 5% CO_2/95% air at 37°C, and the cultured medium was replaced with fresh DMEM containing L-ascorbic acid (50 μg/ml) twice weekly.

Low-intensity pulsed ultrasound stimulation

The sonic accelerated fracture healing system (Exogen Inc., Piscataway, NJ, USA), a LIPUS apparatus, was used to deliver an ultrasound signal. The sonic accelerated fracture healing system is one of the instruments in current clinical use in cases of delayed repair of a fracture. The temporal average intensity was 30 mW/cm² and the frequency was 1.5 MHz with a 200-μs tone burst repeated at 1.0 KHz. LIPUS was applied to the chondrocytes after 24 hours in culture through the bottom of the culture dish (24-well plate) via a coupling gel and silicon rubber that had been placed between the LIPUS transducer and the dish. LIPUS was administered for 20 minutes every day in a span of this experiment. Control samples were prepared in the same manner without LIPUS. Thereafter, the cultured tissues and their supernatant medium were harvested at days 3, 7, 10 and 14.

Cell counting

The cartilage tissues were harvested 1, 3, 7, 10 and 14 days after culture (2 hours after the last LIPUS) and were cut into smaller pieces. Each sample was then incubated for about 8

hours in DMEM (Gibco) supplemented with 0.1% type-II collagenase (Worthington Biochemical Co.), 10%-heat-inactivated FBS (Equitech-Bio, Inc.) and antibiotics. The chondrocytes were then isolated, washed with culture medium, and collected by centrifugation (2,000 rpm, 37°C, 5 min). After the supernatant medium was removed, a solution containing 0.1 M. citric acid and 0.1% crystal violet was added to the cells and then the cells were counted using a hemocytometer (Burker-Turk, Tokyo, Japan).

Histological examinations

Histological evaluations of the specimens were conducted at weeks 1 and 2 post culture. The specimens were fixed overnight in 4% paraformaldehyde in PBS, paraffin-embedded, sectioned to a 5 μm thickness, and were stained with Alcian blue and Safranin O. For each sample, at least two different section levels and two histological sections for each level were analyzed. The sections were analyzed and photographed using an Olympus photomicroscope BX-50 (Olympus Co., Tokyo, Japan).

Immunohistochemistry

Immunohistochemical analyses were conducted with antibodies raised against anti-type-II collagen antibody (1:100; Fuji Pharm. Lab., Toyama, Japan) and against anti-type-IX collagen (1:100; Chemicon International, Billerica, MA, USA) using week 1 and week 2 postcultures to evaluate the expression of the chondrocyte phenotype and also to assess the type-II and type-IX collagen production levels. The specimens from the 1-week and 2-week postcultures that were harvested 2 hours after the last LIPUS were fixed in 4% paraformaldehyde in 0.1 M PBS (pH 7.4), and 16-μm cryostat sections were made.

For further confirmation of chondrocyte growth, Ki67 staining was performed because this factor has been shown to be a very reliable proliferation marker [20]. The monoclonal mouse anti-human antibody Ki67 (MIB1; DAKO, Glostrup, Denmark), which also shows cross-reactivity with porcine tissues, was used to determine the extent of proliferation. The sections cultured at day 7 were incubated with this Ki67 primary antibody, followed by a secondary biotinylated anti-rabbit antibody and horseradish peroxidase–avidin complex (DAKO). The color reaction was developed by 3,3'-diaminobenzidine substrate, followed by counterstaining with hemalaun (Merck, Frankfult, Germany). Chondrocytes showing a definite nuclear staining pattern were scored as positive. All slides were reviewed by two investigators without any prior knowledge of the experiment. Five different randomly chosen areas were reviewed in five different specimens, and the number of Ki67-positive cells per 100 chondrocytes was counted in each slice. The percentages of positive cells (MIB1 index) were then calculated.

Quantitative evaluations were conducted using specimens stained with an anti-β-catenin antibody (Acris, Herford, Germany). The nuclear translocation of β-catenin was visible by brown staining. After counting 100 cells, the ratio of the cells whose nuclei were stained brown was compared between the ultrasound group and the control group. All slides were reviewed by two investigators without any prior knowledge of the experiment. In five different randomly chosen areas in five different specimens, the number of β-catenin antibody-positive stained cells per 100 chondrocytes was counted in each slice. The percentages of positive cells were then calculated.

Western blotting analysis

For the western blotting analysis of the specimens cultured for 1 week, cartilage tissues specimens were harvested 2 hours after the last LIPUS and were cut into smaller pieces. Each sample was then incubated for about 8 hours in DMEM (Gibco) supplemented with 0.1% type-II collagenase (Worthington Biochemical Co.), 10%-heat-inactivated FBS (Equitech-Bio, Inc.) and antibiotics. The chondrocytes were then isolated, washed with culture medium, and collected by centrifugation (2,000 rpm, 37°C, 5 min). After the supernatant medium was removed, the cells were rinsed with 200 μl PBS, filtered by centrifugation, and added to a 200 μl aliquot of 2× sample buffer (62.5 mmol/l Tris–HCl (pH 6.8), 2% SDS, 10% glycerol, 50 mmol/l dithiothreitol, 0.01% bromophenol blue). The cell lysates were then boiled for 10 minutes at 75°C.

Equal amount of the proteins were separated on a 10% SDS–polyacrylamide gel at 200 V, 25 mA for 80 minutes and were transblotted to nitrocellulose membranes (Millipore, Billerica, MA, USA) using a wet transfer system (BIO-RAD, Hercules, CA, USA) at 200 V, 150 mA for 60 minutes. The membranes were blocked with blocking buffer (5% skimmed milk in TBS and 0.05% Tween 20 and Blocking One–P; Nacalai Tesque Inc., Kyoto, Japan) and were incubated with the following antibodies: anti-Akt (Rockland, Gilbertsville, PA, USA), anti-phospho-Akt (Cell Signaling Technology, Beverly, MA, USA), anti-MAPK and anti-phospho-MAPK (Cell Signaling Technology), anti-cyclin D_1 (Biosource, Camarillo, CA, USA), anti-cyclin B_1 and anti-focal adhesion kinase (anti-FAK; Upstate Cell Signaling Solutions, NY, USA), anti-phospho-FAK (Rockland), anti-collagen-II (Chemicon International), and anti-collagen-IX (Cell Signaling Technology).

After incubation with the corresponding horseradish peroxidase-conjugated secondary antibodies (dilution: 1/5,000), membranes were finally incubated with a chemiluminescent reagent (NEL103; Perkin Elmer Life Science, Fremont, CA, USA) and the signals produced were recorded on X-ray film (BIOMAX XAR Film, Rochester, Minesota, USA) for a densitometric analysis. The effects of PI3K inhibitor (LY294002; Cell Signaling Technology) and MEK1 inhibitor (PD98059; Cell Signaling Technology) for cell growth were studied. Chondrocytes were pretreated with MEK1 inhibitor (250 μM/ml) and PI3K inhibitor (250 μM/ml) for 12 hours and 24 hours, followed by stimulation with LIPUS for 20 minutes. Each sample was harvested 2 hours after LIPUS stimulation and the

influence of these inhibitors was judged by western blotting analysis of proliferating cell nuclear antigen (PCNA; DAKO).

Statistical analysis

Data are expressed as the mean ± standard deviation. Quantitative evaluations of Ki67-positive cells and β-catenin-positive cells were assessed by Mann–Whitney's U test. The change in the number of chondrocytes was assessed using repeated-measures analysis of variance. $P < 0.05$ was considered significant.

Results

Histological specimens

After 1 week of culture, cartilaginous tissue consisting of at least five cell layers was formed on the collagen sponges in both the control group and the LIPUS group (Figure 1a to 1d). Simultaneously, both the penetration of chondrocytes and the formation of an extracellular cartilage matrix were observed inside the collagen sponge. In addition, an extracellular matrix rich in proteoglycans and intensively stained with Alcian blue and Safranin O was observed surrounding the chondrocytes.

During week 2 of culture in the 3D system, the cartilaginous tissue in each specimen appeared thicker in comparison with week 1, and the volume of the extracellular matrix had also increased and formed a stable cartilaginous tissue. The thickness of the tissue in week 2 was found to be greater in the LIPUS group than in the control group, and the staining of the matrix, especially near the surface, was also more intense in the LIPUS group (Figure 1e to 1h). The ratio between the number of cells in the cartilage layer that had formed on the collagen sponge and in the sponge was approximately 2:1.

Growth curves of the chondrocytes

The initial results demonstrated that LIPUS facilitates the formation of a 3D structure of cartilage tissue, suggesting that increased cell proliferation had occurred. The effect of LIPUS on cell proliferation was therefore examined in the culture system. The number of live chondrocytes on day 0 was $(13.6 \pm 0.8) \times 10^5$ and $(12.9 \pm 0.6) \times 10^5$ cells in the control and LIPUS groups, respectively. A time-dependent increase in the total number of chondrocytes was noted, and on day 14 the cell counts were $(30.4 \pm 0.8) \times 10^5$ and $(33.0 \pm 1.7) \times 10^5$ in the control group and the LIPUS group, respectively. There was therefore a small but significantly greater increase in the cell number observed in the LIPUS group in comparison with the control group ($P < 0.01$; Figure 2).

Type-II collagen and type-IX collagen

Collagen is essential for the formation of cartilage tissue and also for the proliferation of chondrocytes. Furthermore, the current results demonstrated the formation of a thicker cartilaginous structure following LIPUS – suggesting that the increased secretion of extracellular matrix components such as the collagens had occurred.

Figure 1

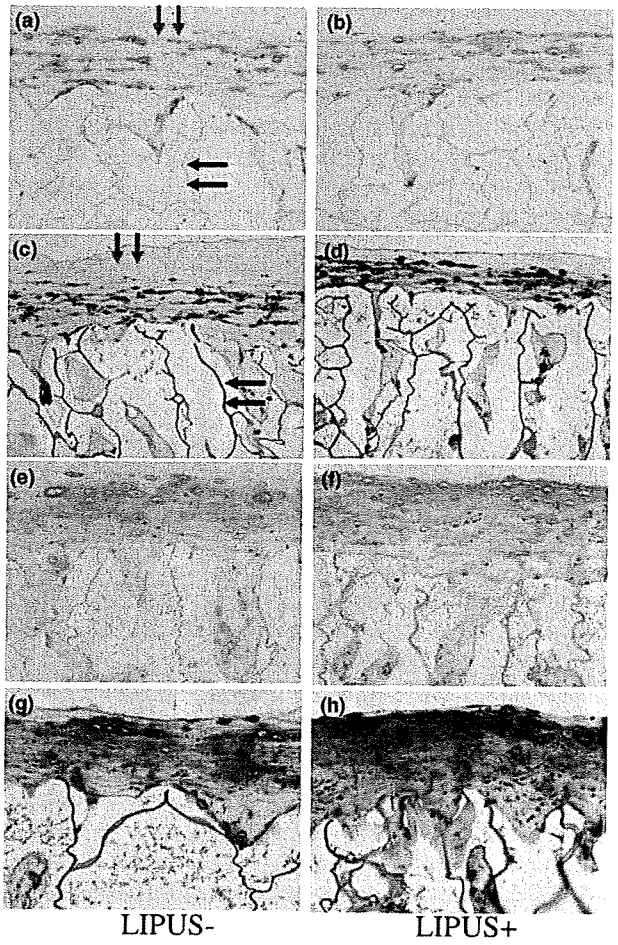

High-magnification sections of chondrocyte–collagen sponges 1 week after culture. Cartilage layers with a laminar structure on the collagen sponges (green arrows) and a grey structure, which represents the walls of collagen sponges (black arrows), are visible at high magnification (100×). **(a)** to **(d)** Specimens at week 1 of culture. (a) and (b) Alcian blue staining, and (c) and (d) Safranin O staining: many chondrocytes with blue-stained and red-stained peripheral matrices could be observed, respectively. The chondrocytes exhibited a layer structure, and their infiltration into the sponge can also be observed. **(e)** to **(h)** Specimens at week 2 of culture. (e) and (f) Alcian blue staining, and (g) and (h) Safranin O staining: many chondrocytes with blue-stained and red-stained peripheral matrices can be observed, respectively. The layer of chondrocytes that formed on the surface of the sponge was found to be thicker in comparison with the week 1 cultures, and the volume of the extracellular matrix had also increased. The cartilage tissue that formed on the surface of the sponge consisted of more than 10 layers of chondrocytes. The staining of the extracellular matrix in the LIPUS group was also found to be stronger than in the control group.

Following type-II collagen antibody staining, both the chondrocyte layers, which formed cartilaginous tissue on the collagen sponge, and the matrix formed inside the sponge were strongly positive in both the LIPUS group and the control group. There were also no apparent differences in the

Figure 2

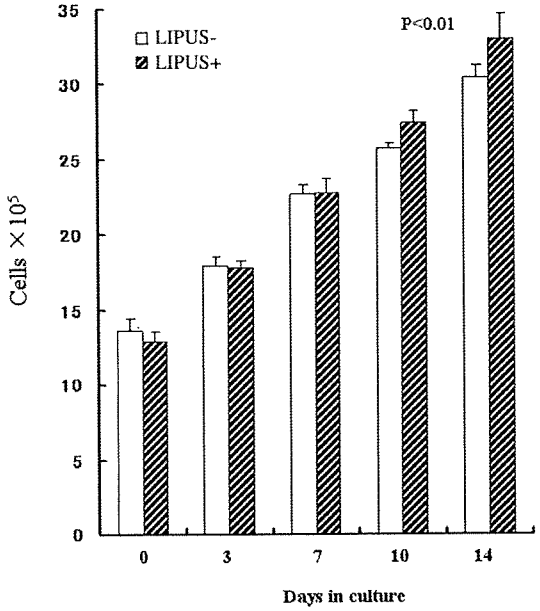

Growth curves of the cells in the chondrocyte–collagen sponges (n = 7). A time-dependent increase in the number of chondrocytes can be seen in both the low-intensity pulsed ultrasound (LIPUS) group (US+) and in the control group (US-). The rate of increase in the chondrocytes number was significantly greater, however, in the LIPUS group in comparison with the control group ($P < 0.01$). The change in the number of chondrocytes was assessed using repeated-measures analysis of variance.

intensities of this staining between these two groups (Figure 3a to 3d).

Type-IX collagen antibody staining of the culture specimens showed the intensity of this staining in the chondrocyte layers on the sponge to be far stronger in the LIPUS group than in the control group after 2 weeks of culture, thus indicating an accumulation of type-IX collagen (Figure 3e to 3h).

Ki67 and β-catenin

Immunohistochemical staining with Ki67 revealed distinctive labeling in the chondrocyte nuclei (Figure 4a,b). The cells with brown-stained nuclei were considered Ki67-positive. The large number of Ki67-positive cells indicated that LIPUS stimulated cell proliferation. In the cells in which β-catenin had translocated to the nucleus, brown nuclear staining with an anti-β-catenin antibody was evident (Figure 4c,d).

Quantitative evaluation of both Ki67-positive cells and β-catenin-positive cells

The Ki67 index of the chondrocytes exposed to LIPUS was found to be 48 ± 3.7%, in comparison with 41 ± 3.0% in the control group (Figure 5a), which was significantly different. The average percentage of β-catenin-positive cells with brown-stained nuclei (that is, positive cells) was determined to

Figure 3

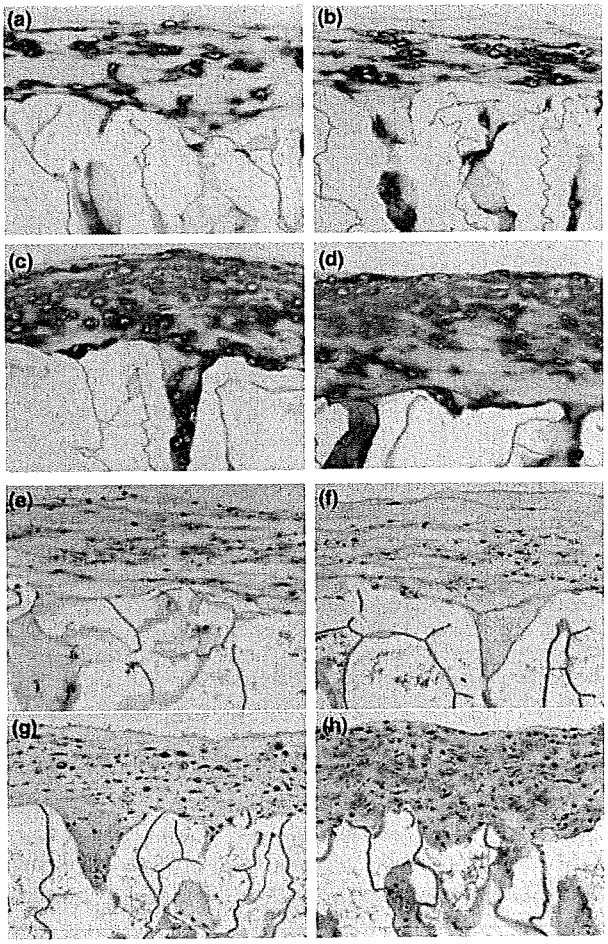

High-magnification sections of chondrocyte–collagen sponges 1 and 2 weeks post culture. Sections of chondrocyte–collagen sponges 1 and 2 weeks post culture at high magnification (anti-collagen antibody type-II and type-IX stain, 100×). **(a)**, **(b)** Anti-type-II collagen antibody staining of specimens after week 1 of culture. Brown staining of the matrix with anti-collagen type-II antibodies can be observed around the chondrocytes, indicating production of this collagen. **(c)**, **(d)** Anti-type-II collagen antibody-stained specimens after week 2 of culture. Strong brown staining of the matrix can be observed around the cells at a similar level in both groups. **(e)**, **(f)** Anti-type-IX collagen antibody-stained specimens after week 1 of culture. Positive brown staining of the matrix with anti-type-IX collagen antibodies can be observed around the cells, thus indicating the production of this collagen around the chondrocytes. **(g)**, **(h)** Anti-type-IX collagen antibody stained specimens after week 2 of culture. Positive brown staining of the matrix with anti-type-IX collagen antibodies can be observed around the cells, thus indicating production of this collagen around the chondrocytes.

be 42 ± 4.9% in the LIPUS group and 32 ± 2.7% in the control group. This indicated a significant difference between the two groups (Figure 5b).

Figure 4

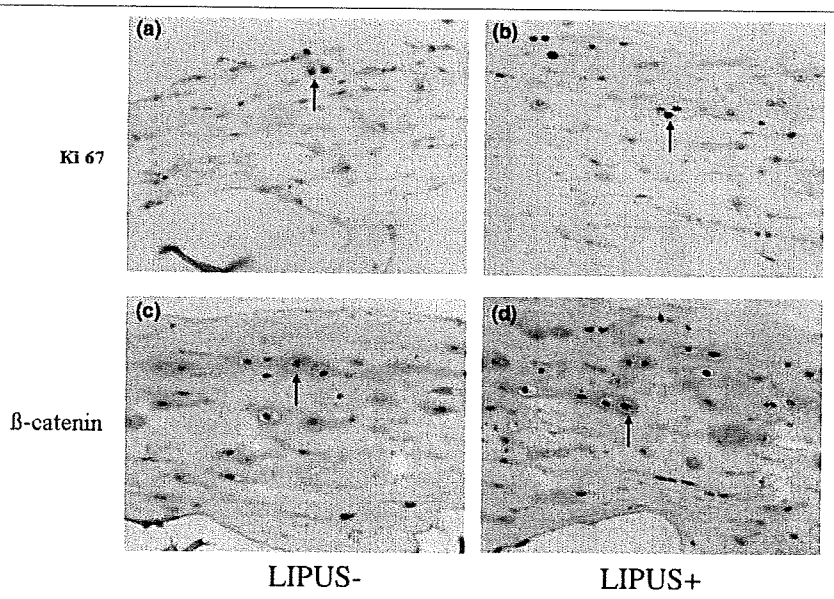

Ki67 and β-catenin antibody staining. (a), (b) Anti-Ki67 antibody staining of week 2 cultures (200× magnification). The nuclei are positively stained with an anti-Ki67 antibody in both the control group (US-) and the low-intensity pulsed ultrasound (LIPUS) group (US+) (black arrows). **(c), (d)** Anti-β-catenin antibody staining of week 2 cultures (200× magnification). The nuclei are positively stained with an anti-β-catenin antibody in both the control group (US-) and the LIPUS group (US+) (black arrows).

Western blotting analysis

Collagen type-II

A western blot analysis showed immunoreactive bands for collagen type-II were observed at about 200 kDa, and were found to be present at a similar intensity in the LIPUS group and the control group (Figure 6a).

Collagen type-IX

An immunoreactive western band for collagen type-IX of about 110 kDa was detected at a higher level in the LIPUS group in comparison with the control group (Figure 6b).

FAK, phosphorylated FAK, Paxillin and phosphorylated Paxillin

Immunoreactive bands corresponding to FAK and phosphor-

Figure 5

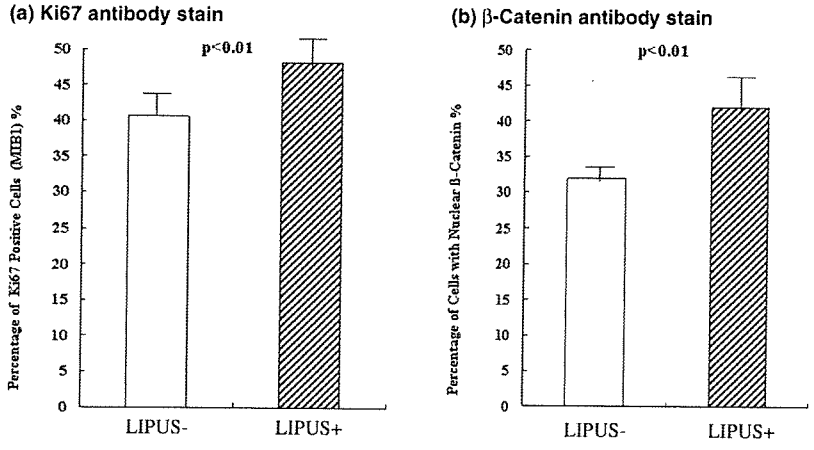

Quantitative evaluation of Ki67-positive cells and β-catenin-positive cells. After counting 100 cells in each specimen in the low-intensity pulsed ultrasound (LIPUS) group (US+) and the control group (US-), the numbers of cells with positively stained nuclei were compared for both **(a)** Ki67 and **(b)** β-catenin. There were significantly more brown stained cells in the LIPUS group in both cases ($P < 0.01$).

ylated FAK were detected by western blotting at about 125 kDa (Figure 6c). Positive bands for Paxillin and its phosphorylated form were observed at about 68 kDa (Figure 6d). Although the levels of total FAK and Paxillin were similar with and without LIPUS exposure, the staining of their phosphorylated counterparts was stronger in the LIPUS group than in the control group (Figure 6c,d). These data thus indicate that LIPUS exposure results in the activation of both FAK and Paxillin.

MAPK and phosphorylated MAPK
Whereas MAPK and phosphorylated MAPK (p-42, p-44) were both detected in both the LIPUS group and the control group, there were no evident differences in the intensity (Figure 6e).

Akt and phosphorylated Akt
Akt, a cell survival signal, was found to be similarly expressed in both the LIPUS group and the control group but was observed to be phosphorylated to a greater extent in the LIPUS group (Figure 6f). These results indicate that LIPUS increased cell proliferation in this culture system by preferentially activating the PI3K/Akt pathway rather than the MEK/MAPK pathway.

Cyclin B_1 and cyclin D_1
Consistent with the increased chondrocyte growth, the expression of the cell proliferation markers cyclin D_1 and cyclin B_1 was enhanced in both cases by LIPUS. The expression of both of these cyclins was also detected at higher levels in the LIPUS group in comparison with the control group (Figure 6g). These results confirm that the increase in cell numbers in response to LIPUS coincide with the enhanced expression of these two cyclins.

Changes of proliferating cell nuclear antigen using MEK1 inhibitor and PI3K inhibitor
The influence of the MEK1 inhibitor (PD98059) and of the PI3K inhibitor (LY294002) was judged in western blotting analysis of PCNA. The expression of PCNA at 12 hours was decreased by PD98059 in the LIPUS-negative group and was detected at higher level in the LIPUS-positive group in comparison with the LIPUS-negative group, but the expression of PCNA at 24 hour was completely decreased by this inhibitor in both the LIPUS-negative and LIPUS-positive groups. Cell growth according to LIPUS is hypothesized to depend not only on a MAPK cascade but also on the effect of other signal transductions. The expression of PCNA at 12 and 24 hours, however, was completely decreased by PI3K inhibitor (LY294002).

Discussion

LIPUS promotes proliferation of chondrocytes

Previous studies indicated that LIPUS increases the production of the extracellular matrix around chondrocytes, but not the actual proliferation of the chondrocytes themselves. Zhang and colleagues have reported that although pulsed low-intensity ultrasound increases the number of hypertrophic chondrocytes around the callus of healing fractures, it does not alter the hyaline cartilage [15]. Nishikori and coworkers have also reported that chondrocytes can be grown in a 3D collagen gel without loss of their chondrogenic phenotype but that LIPUS did not enhance cell proliferation in either a monolayer culture or a 3D culture [13]. In this same study, ultrasound exposure was found to be advantageous in inducing chondrocyte production of collagen gel composites with mature aggrecan.

Parvizi and colleagues irradiated the rat monolayer culture cells at 1 MHz to investigate the [^{3}H]thymidine incorporation levels, the DNA contents, the mRNA levels of α(I) and α(II) procollagens and the mRNA contents of proteoglycans inducing aggrecan. The group reported that the irradiation increased the aggrecan mRNA and proteoglycan levels without any significant effects upon the proliferation of chondrocytes [14].

A number of studies have reported a slight increase in the number of chondrocytes following the use of the same therapeutic low-intensity pulsed ultrasound, which may be called PLIUS. Zhang and colleagues previously irradiated cultured chondrocytes at 2 mW/cm^2 and 30 mW/cm^2, and measured the cell count and volume of the extracellular matrix over time. At 2 mW/cm^2, they reported that the extracellular matrix as well as the cell number increases significantly but only transiently on day 3 of culture, in comparison with the control group [15]. In the current study with a 3D culture system, the number of chondrocytes doubled by the end of the 2-week incubation in both groups. This rate of increase was slightly but significantly higher in the LIPUS group.

To further confirm these findings, Ki67 staining of sections from these cultures was performed because it has been shown to be a very reliable proliferation marker. The Ki67 index in the LIPUS group, also significantly higher in comparison with the control group, again indicated that LIPUS promotes the proliferation of chondrocytes slightly but significantly. In terms of cartilage regeneration, even a slight increase in the number of chondrocytes is very important. In a previous study performed *in vivo* by Cook and colleagues, cartilage defects in New Zealand rabbits were artificially induced by drilling holes. These defects treated by LIPUS regenerated articular cartilage earlier than the control group, with a hint of increased numbers of chondrocytes [21]. In many previous *in vitro* studies, the cartilage of small animals such as mice and rats has been used. Chondrocytes in cartilage of these animals have a tendency to proliferate more easily, and therefore the regeneration of cartilage is easier than in higher animals. The current study utilized porcine cartilage on the assumption that this is a more appropriate animal model system for the development of future treatments in human cartilage.